

# MOUNTAIN-PLAINS CONSORTIUM

MPC 22-479 | M. Farhadmanesh, C. Cross, and A. Rashidi

## IMAGE-BASED 3D RECONSTRUCTION OF UTAH ROADWAY ASSETS



A University Transportation Center sponsored by the U.S. Department of Transportation serving the Mountain-Plains Region. Consortium members:

Colorado State University  
North Dakota State University  
South Dakota State University

University of Colorado Denver  
University of Denver  
University of Utah

Utah State University  
University of Wyoming

**Technical Report Documentation Page**

1. Report No. MPC-606		2. Government Accession No.		3. Recipient's Catalog No.	
4. Title and Subtitle  Image-Based 3D Reconstruction of Utah Roadway Assets				5. Report Date August 2022	
				6. Performing Organization Code	
7. Author(s)  Mohammad Farhadmanesh, Chandler Cross, and Dr. Abbas Rashidi				8. Performing Organization Report No.  MPC 22-479	
9. Performing Organization Name and Address  Department of Civil & Environmental Engineering The University of Utah 201 Presidents' Cir. Salt Lake City, UT 84112				10. Work Unit No. (TRAIS)	
				11. Contract or Grant No.	
12. Sponsoring Agency Name and Address  Mountain-Plains Consortium North Dakota State University PO Box 6050, Fargo, ND 58108				13. Type of Report and Period Covered  Final Report	
				14. Sponsoring Agency Code	
15. Supplementary Notes Supported by a grant from the US DOT, University Transportation Centers Program					
16. Abstract  Understanding the condition of roadway assets is important for transportation agencies to plan for future improvements and asset management purposes quantitatively. Since these assets are distributed across the country, a manual data collection system falls short of the automated methods due to time and cost issues. Some pioneer departments of transportation in the United States use mobile Light Detection and Ranging (LiDAR) to monitor highway assets and pavement condition data. However, LiDAR is expensive and not affordable for every maintenance agency. Additionally, special technical knowledge is required to perform this method, which may not be accessible to the maintenance agency staff. Recently, image-based 3D reconstruction has been shown to be a cheaper and simpler technology than LiDAR. In this report, we assess the alternative method (image-based) for reconstructing 3D models (virtual 3D point clouds) of transportation agencies. The analysis of the data quality and associated costs holds the promise for conducting a feasible roadway asset inventory.					
17. Key Word  asset management, data collection, evaluation and assessment, feasibility analysis, highways, laser radar, photogrammetry, software				18. Distribution Statement  Public distribution	
19. Security Classif. (of this report) Unclassified		20. Security Classif. (of this page) Unclassified		21. No. of Pages 55	22. Price n/a

# **Image-Based 3D Reconstruction of Utah Roadway Assets**

Mohammad Farhadmanesh

Chandler Cross

Dr. Abbas Rashidi

Department of Civil & Environmental Engineering  
The University of Utah  
Salt Lake City, Utah

August 2022

## **ACKNOWLEDGMENTS**

This project is funded by the Utah Department of Transportation (UDOT) and Mountain-Plains Consortium (MPC). The opinions and findings of the authors do not necessarily reflect the view and opinions of UDOT and MPC.

## **DISCLAIMER**

The contents of this report reflect the views of the authors, who are responsible for the facts and the accuracy of the information presented. This document is disseminated under the sponsorship of the Mountain-Plains Consortium, in the interest of information exchange. The U.S. Government assumes no liability for the contents or use thereof.

NDSU does not discriminate in its programs and activities on the basis of age, color, gender expression/identity, genetic information, marital status, national origin, participation in lawful off-campus activity, physical or mental disability, pregnancy, public assistance status, race, religion, sex, sexual orientation, spousal relationship to current employee, or veteran status, as applicable. Direct inquiries to Vice Provost, Title IX/ADA Coordinator, Old Main 201, [\(701\) 231-7708](tel:7012317708), [ndsuoaaa@ndsuo.edu](mailto:ndsuoaaa@ndsuo.edu).

## **ABSTRACT**

Understanding the condition of roadway assets is important for transportation agencies to plan for future improvements and asset management purposes quantitatively. Since these assets are distributed across the country, a manual data collection system falls short of the automated methods due to time and cost issues. Some pioneer departments of transportation in the United States use mobile Light Detection and Ranging (LiDAR) to monitor highway assets and pavement condition data. However, LiDAR is expensive and not affordable for every maintenance agency. Additionally, special technical knowledge is required to perform this method, which may not be accessible to the maintenance agency staff. Recently, image-based 3D reconstruction has been shown to be a cheaper and simpler technology than LiDAR. In this report, we assess the alternative method (image-based) for reconstructing 3D models (virtual 3D point clouds) of transportation agencies. The analysis of the data quality and associated costs holds the promise for conducting a feasible roadway asset inventory.

# TABLE OF CONTENTS

<b>1. INTRODUCTION</b> .....	<b>2</b>
1.1 Introduction.....	2
1.2 Current Gap In Study.....	3
1.3 Performance Measurement.....	5
<b>2. BACKGROUND</b> .....	<b>8</b>
2.1 LiDAR Technology.....	8
2.2 Image-Based 3D Reconstruction Technology.....	9
2.3 Automated 3D Modeling in Other Industries.....	10
<b>3. METHODOLOGY</b> .....	<b>12</b>
3.1 Mobile (Vehicular) Data Collection.....	12
3.1.1 Mobile LiDAR.....	12
3.1.2 Mobile Photogrammetry.....	12
3.2 Terrestrial Data Collection.....	17
3.2.1 Terrestrial LiDAR.....	17
3.2.2 Terrestrial Photogrammetry.....	18
<b>4. ASSESSMENT METRICS</b> .....	<b>21</b>
4.1 Quality and Accuracy Metrics for Mobile Procedures.....	21
4.2 Quality and Accuracy Metrics for Terrestrial Procedures.....	22
<b>5. RESULTS</b> .....	<b>26</b>
5.1 Software Packages Comparison.....	26
5.2 Results of the Mobile Collected 3D Data.....	26
5.2.1 Roadway Assets (Traffic Signs).....	26
5.2.2 Pavement.....	33
5.2.3 Bridge.....	34
5.3 Results of the Terrestrial Collected 3D Data.....	37
5.3.1 Pedestrian Access Ramp.....	37
<b>6. CONCLUSIONS</b> .....	<b>43</b>
6.1 Challenges and Limitations.....	44
6.2 Recommendations.....	44
<b>REFERENCES</b> .....	<b>46</b>

## LIST OF TABLES

Table 3.1	Mobile data collection details.....	15
Table 3.2	Terrestrial data collection details.....	20
Table 5.1	Comparison of different software packages using a control set of 163 images .....	26
Table 5.2	Data collection and processing for asset management models.....	27
Table 5.3	Measurement overview of image-based and LiDAR-based point clouds for asset management.....	28
Table 5.4	Model 1 Traffic Sign Details.....	29
Table 5.5	Extracted Bridge Span Measurements for Terrestrial and Mobile LiDAR-based Reconstruction.....	37
Table 5.6	Pedestrian access ramp slope errors .....	38
Table 5.7	Data Processing Table for Pedestrian Access Ramps .....	39

## LIST OF FIGURES

Figure 1.1	3D models (point cloud) of as-built infrastructure.....	2
Figure 1.2	Mobile LiDAR for roadway asset data collection (Mandli Communication setup) .....	4
Figure 1.3	Linear accuracy evaluation .....	6
Figure 1.4	Slope measurement in created 3D models .....	6
Figure 2.1	Different types of laser scanners .....	8
Figure 2.2	Image-based 3D reconstruction; The Structure from Motion (SfM) technique .....	9
Figure 2.3	3D modeling of constructed structures.....	11
Figure 3.1	Mandli mobile LiDAR data collection setup (version X-35).....	13
Figure 3.2	GoPro Mounted on a vehicle.....	14
Figure 3.3	Different mounting areas and the corresponding view on the bottom .....	17
Figure 3.4	Maptek I-Site 8820 terrestrial LiDAR .....	18
Figure 3.5	Fujifilm XT-30 mirrorless digital camera .....	19
Figure 3.6	Circular pattern for image acquisition.....	19
Figure 4.1	Dense point cloud model vs sparse point cloud model .....	21
Figure 4.2	Super imposed facets for measurements of the traffic sign edges .....	22
Figure 4.3	Pedestrian Access Ramp Components. Red: Pedestrian Access Route (PAR), Blue: Turning Space (T), Yellow: Ramp, Purple: Flares, Green: Detectable Warning Surface (DWS), Light Blue: Clear Space, Orange: Crosswalk.....	23
Figure 4.4	Smart Tool Smart level .....	24
Figure 4.5	Slope measurement of a flare component of a pedestrian access ramp. $\Delta Z$ is the change in elevation, $\Delta XY$ is the projected distance along the XY plane.....	24
Figure 5.1	The photogrammetric point cloud for model 1; (a) Density histogram (number of neighbors); (b) Model Saturation (red: the most saturated part, blue: the lowest saturated part).....	30
Figure 5.2	The LiDAR point cloud for model 1; (a) Density histogram (number of neighbors); (b) Model Saturation (red: the most saturated part, blue: the lowest saturated part) .....	30
Figure 5.3	The photogrammetric point cloud for model 2; (a) Density histogram (number of neighbors); (b) Model Saturation (red: the most saturated part, blue: the lowest saturated part).....	31
Figure 5.4	The LiDAR point cloud for model 2; (a) Density histogram (number of neighbors); (b) Model Saturation (red: the most saturated part, blue: the lowest saturated part) .....	31
Figure 5.5	The photogrammetric point cloud for model 3; (a) Density histogram (number of neighbors); (b) Model Saturation (red: the most saturated part, blue: the lowest saturated part).....	32
Figure 5.6	The LiDAR point cloud for model 3; (a) Density histogram (number of neighbors); (b) Model Saturation (red: the most saturated part, blue: the lowest saturated part) .....	32



Figure 5.7	Camera field-of-view of the hood-mounted camera .....	33
Figure 5.8	(Bottom) Parking area point cloud, (above) Target pavement distress point-cloud (modeled using LiDAR) to point-cloud (modeled using photogrammetry) (C2C) absolute distances (distances unit in centimeter) .....	34
Figure 5.9	The target bridge .....	35
Figure 5.10	Map of reconstructed highway sections (showing the bridge model and a traffic sign model). Images are from both LiDAR-based highway models and image-based highway models .....	36
Figure 5.11	Bridge's underside in (a) Mobile photogrammetry model, (b) Mobile LiDAR model, (c) Terrestrial LiDAR model.....	37
Figure 5.12	Ramp 1 point clouds using (a) photogrammetry and (b) LiDAR.....	40
Figure 5.13	Comparison of UDOT's in-field measurements to measurements extracted from image-based point clouds for Ramp 1. (a) & (b) UDOT C-170 evaluation form, (c) extracted measurements vs. UDOT's measurements.....	41

## EXECUTIVE SUMMARY

Roadway assets are scattered on a large scale across the country. As a result, monitoring the condition and statistics of the existing assets is a huge problem for asset management divisions at transportation agencies. Manual data collection systems have been outdated for a long time as automated technologies emerged. Recently, some pioneer departments of transportation (DOTs), such as Utah DOT, have leveraged LiDAR technology as a tool for their asset inventory. Using this technology, DOTs can have access to 3D point cloud models of the assets' data, thereby providing them with valuable information, such as assets' as-is conditions and their geospatial data. However, LiDAR is expensive and difficult to use for untrained staff. On the other hand, photogrammetry offers a more affordable solution and is easy to apply, considering the recent availability of image-based 3D reconstruction commercial software packages. This technology uses digital images and their overlap to calculate the depth information and reconstruct the scenes in the form of a point cloud similar to the LiDAR output.

In this project, we evaluated the feasibility of photogrammetry as an asset management tool for transportation agencies. This report elaborates on our conducted research in doing so. Considering the accuracy requirement for collecting different transportation assets, we tested two different data collection procedures: mobile and terrestrial data collection. The former helps us collect assets distributed across the roadways, such as overhead and roadside traffic signs, highway bridges, and pavement. The latter is suitable for cases such as pedestrian access ramps, which require accurate 3D reconstruction due to the inspection standards. The mobile procedures are conducted using a vehicular platform carrying the sensors (i.e., laser scanner and digital cameras). Laser scanners immediately produce the 3D point cloud models, requiring large data storage capacities. Digital images captured by cameras are stored and processed later in an office to create similar 3D models using an advanced technique named Structure from Motion (SfM). Handheld digital cameras are used to take the necessary images in a circular pattern for terrestrial procedures.

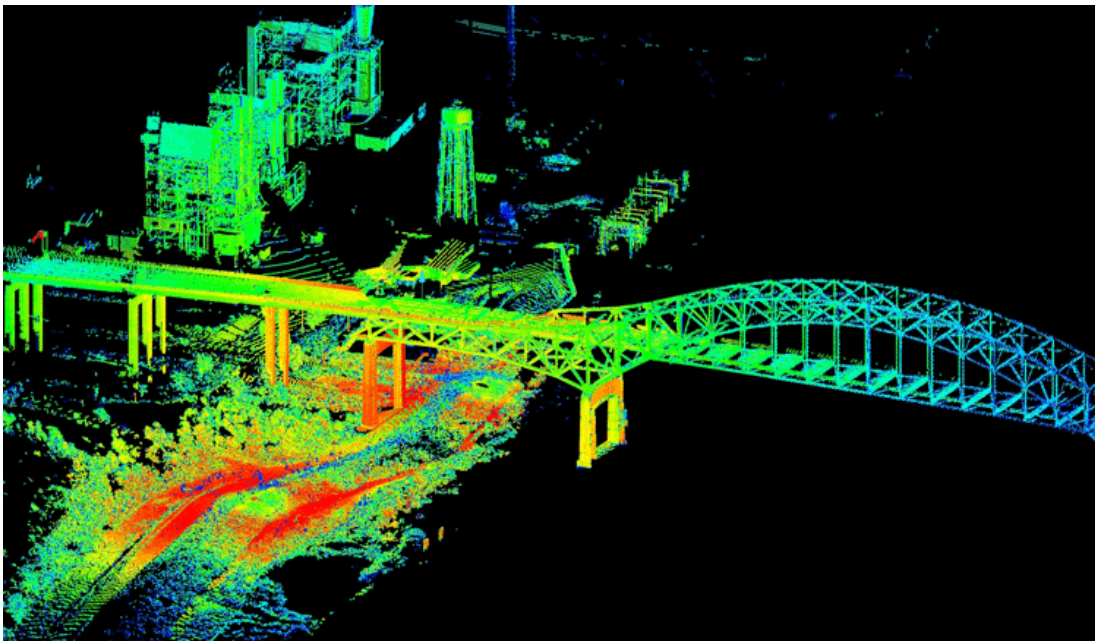
Evaluation of quality and accuracy of the produced models has revealed useful information. Standard quality and accuracy metrics showed that image-based 3D reconstruction could be used as an alternative solution for remote inspection of pedestrian access ramps, since it is cheaper and accurate enough. According to the bridge case study, mobile LiDAR is the current superior technology for highway asset inventorying but is not detailed enough to be used as a tool for structural highway bridge inspections. Moreover, photogrammetry can only work well as a reliable alternative to LiDAR technology in favorable lighting and illumination condition (e.g., no sudden change in illumination) for the highway asset inventory system. Additionally, mobile photogrammetry works well in cases where the camera platform can be moved at slower speeds (slower than approximately 50 miles per hour), and the assets are not far from the roadway (less than two lanes far away). LiDAR may be the better technology for faster rates of travel and assets at farther distances. Considering overall point cloud densities results in the first case study and point cloud deviation measurements in the second case study, the authors recommend the use of photogrammetry for pavement distress analysis only on the road lane in which the mobile sensor is located (the lane that the vehicle is located).

# 1. INTRODUCTION

## 1.1 Introduction

Constant maintenance is one of the top priorities of the U.S. Department of Transportation [1]. The meaning of roadway maintenance is to keep its assets and facilities as close as possible to the condition as they were once constructed [2]. For that reason, asset inventory divisions need a complete list of the existing assets and facilities to compare them with their as-built version and evaluate the current state of the roadway conditions. Furthermore, they need such data for fair allocation of national funds to different areas and agencies across the country [3]. Other applications are traffic and capacity engineering, federal and state planning, budgetary allocation, and budget request justification. During the past years, transportation agencies have leveraged modern technologies to build roadway assets.

Two of those technologies are Light Detection and Ranging (LiDAR) and photogrammetry. These technologies can help transportation agencies automate the process of asset data acquisition across roadways (streets and highways). The laser-scanning technology leverages millions of laser light pulses to virtually scan and build a 3D model of roadways (Figure 1.1). To build the 3D model, the LiDAR calculates the time that it takes for the light pulse to get to the object in the roadways and return to the laser sensor, and using time-of-flight principles, it measures the distance of each scanned point in the roadways.



**Figure 1.1** 3D models (point cloud) of as-built infrastructure

The other emerging technology is photogrammetry. This image-based technology leverages 2D digital images to build the digital 3D models of the scenes that are in those digital images. Currently, many transportation agencies carry out their roadway data collection using LiDAR. Examples of those pioneers in using the LiDAR technology are the Massachusetts Department of Transportation and the Utah Department of Transportation (UDOT) [4,5].

When using laser-scanning technologies, such as LiDAR, it is important to note that this technology produces accurate 3D models in the form of point clouds. However, the cost of the use of this technology is very high. LiDAR technology is expensive because of its expensive equipment. On the other hand, photogrammetry costs much less than LiDAR technology and also has shown comparable accuracy for many engineering applications. This is due to the recent advances in computer science and the development of the software packages that bring the technology of image-based 3D reconstruction to the access of the public and not just researchers.

The photogrammetry technology is considerably cheaper than LiDAR and requires less training to operate. The problem with the photogrammetry technology is that we need to verify the accuracy and feasibility of this technology for the case at hand. Many factors are yet to be assessed before accepting this technology as a feasible method and alternative to LiDAR technology. Those factors are image qualities and resolutions, lighting conditions, number of provided images, and image overlap percentage. Also, different roadway maintenance divisions need various levels of accuracy and quality in their asset inventory data. That said, this project conducts a feasibility research study for leveraging photogrammetry to compile different roadway asset inventories. It helps transportation agencies with consideration of their budget to choose the appropriate technology for their use.

This report studied the applicability of using photogrammetry in three roadway asset maintenance applications: 1. Highway bridges and traffic sign asset assessment; 2. Pedestrian access ramps; and 3. Pavement condition assessment. This report discusses the advantages, disadvantages, and limitations of photogrammetry and finishes with implementation recommendations.

In this work, we first reviewed the two applied 3D-reconstruction methods — photogrammetry and LiDAR technologies. Next, we reviewed the conducted research works in roadway assets condition and pavement condition assessment using spatial data generated by either active sensor-based technique (laser scanning) or passive sensor-based technique (photo/videogrammetry). In the data collection section, we conducted in-field case studies to evaluate the feasibility of using photogrammetry in roadway asset management and pavement condition assessment. Finally, recommendations, limitations, and benefits are discussed in the conclusion section.

## **1.2 Current Gap In Study**

Many of the current transportation agencies that are using LiDAR technology trust this technology for its promising accuracy in the collection of the 3D data of the built environment. The fact that LiDAR produces accurate point cloud models reduces the risk factor for using this technology. However, to choose an alternative solution, these agencies cannot make a sensible decision unless they know whether that technology can meet their requirements or not. The main reason for the use of LiDAR technology by the Utah Department of Transportation and some other DOTs is also the same as stated above (Figure 1.2) [6].

The extravagant cost of the LiDAR technology does not allow all transportation agencies (especially small-sized transportation agencies) to use this automated technology and provide their transportation planners with accurate inventory data of the roadways in their jurisdiction. Therefore, there has been a debate over the use of photogrammetry in transportation agencies that cannot afford LiDAR technology. Also, photogrammetry, if applicable, can reduce a large number of costs at larger transportation agencies if it replaces the LiDAR technology for the task of roadway asset data collection and asset inventory.

It is important to note that the required accuracy and quality for different applications in the abovementioned transportation agencies may vary from high to low. Those applications are asset management, maintenance, and structural inspection of those assets.

Therefore, engineers need to have a quantitative understanding of the accuracy that the two 3D reconstruction technologies can provide for them. That said, conducting a comparison between the point clouds generated by laser scanners and the point clouds generated by photogrammetry is the exact research needed to make an educated decision on which technology is a better fit for the task at hand. In addition, the accuracy and quality level that any sensor-based (including LiDAR and photogrammetry) technology provides highly depend on all the settings in which they are applied.



**Figure 1.2** Mobile LiDAR for roadway asset data collection (Mandli Communication setup)

There are a few factors that can affect the quality and accuracy of the collected data by LiDAR and photogrammetry technologies. One of those factors is the speed of the moving platform that is being used to carry the sensors (laser scanner sensor in the case of LiDAR and digital camera sensors in the case of photogrammetry).

According to an extensive review of research, there is a lack of research in photogrammetry-based point clouds and scanner-based point clouds taken by moving sensors (scanners and digital cameras) at different speeds. This motion during the action of the data collection may introduce some blurry effects on the captured digital images by the digital camera sensors. The blurry effect also reduces the total number of valid image features between the sequence of the images when using a photogrammetry software package.

Likewise, due to being mobile during the data collection of the roadways, even the expensive, modern scanners (LiDAR units) are not able to operate at such high accuracy that they normally can operate in stationary settings. Therefore, we have divided our field test studies into three categories that are common in transportation applications as follows:

1. Roadway asset management and maintenance
2. Pedestrian ramp inspection
3. Pavement condition assessment

The above categories have been chosen due to the various speeds of the in-motion sensors used during the data acquisition process. For the first category (i.e., roadway asset management and maintenance), we collected data in two sub-categories of data collection. We collected and analyzed the collected separately for highways and city streets. The first sub-category (highway data collection) required us to move the platform at a higher speed than the speed of the platform when used for the second sub-category case (city streets data collection).

The data for pedestrian inspection is captured and recorded in a semi-stationary and fully-stationary setting. In addition to the accuracy and quality assessment of the above categories, the cost and efficiency of the two data-acquisition approaches are evaluated. Each category would require a different set of equipment, resulting in completely different costs for the associated transportation agencies.

Furthermore, new advances in the software packages accessible to the public, including the photogrammetry-enabled software packages, have modified the path where an engineer can build the 3D models of their targeted facility or object. These available software packages used to be in the form of open-source computer programs and for research purposes only. Still, because of their different algorithms in processing and providing the final output, non-expert users need guidance in choosing their desired software package appropriate to their application.

Because of the data collection challenges in the area of transportation engineering, the same images can result in different outputs if different software packages are used. Because of that, our research team decided to demonstrate the results of different software packages that are used in the same location and facility to evaluate the feasibility of those software packages in the above-mentioned transportation applications.

In addition, these fast-prepared 3D representations could also help project managers to document existing assets on their sites. Thus, in this paper, we also worked on giving a realistic assessment of the time of data-collection and data-processing for each of the different mentioned tasks to help the decision-makers employ one of these technologies in their projects.

Since we are aware that the accuracy of the LiDAR and photogrammetry technologies is sensitive to weather conditions, we investigated the accuracy and quality of the produced data in different weather conditions, including favorable and unfavorable weather conditions. The included unfavorable weather conditions are rainy, snowy, and stormy. These weather conditions affect the reflectivity of the target surfaces (traffic signs, bridge surfaces, pavements, etc.). The favorable weather conditions included sunny and cloudy days.

### **1.3 Performance Measurement**

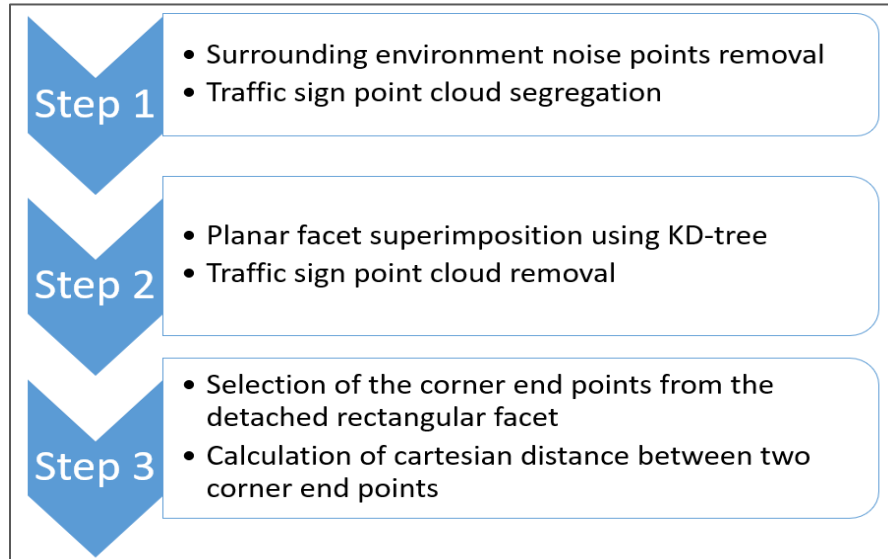
Although the data format for both LiDAR and photogrammetry are the same (point cloud models), the accuracy for the reconstructed models may differ. Parameters, such as the density of generated point clouds, should be evaluated to assess the quality of the point cloud models.

Despite the growing popularity of close-range photogrammetry and its ease of use and low-cost technology, it has not yet been considered a practical scanning tool within divisions in transportation agencies. This project and report aim to address this issue and explore the feasibility of using close-range photogrammetry as an alternative technology to the currently used LiDAR technology at transportation agencies.

To quantitatively characterize the quality of the point clouds resulting from both ultra-light laser scanners and digital cameras, we have improvised standard measurements for each one of the mentioned transportation application categories [7]. The first standard accuracy metric considered for this project is the linear accuracy in reconstructing the 3D models. We measure this metric by comparing the ratios of the length to the width of the reconstructed planar objects.

The value of these ratios obtained from assessing both photogrammetric and LiDAR-based models will be compared to each other to find the most accurate method and the level of the accuracy of the method that offers less accuracy. We used an algorithm named k-dimensional trees [8] to superimpose a facet to the

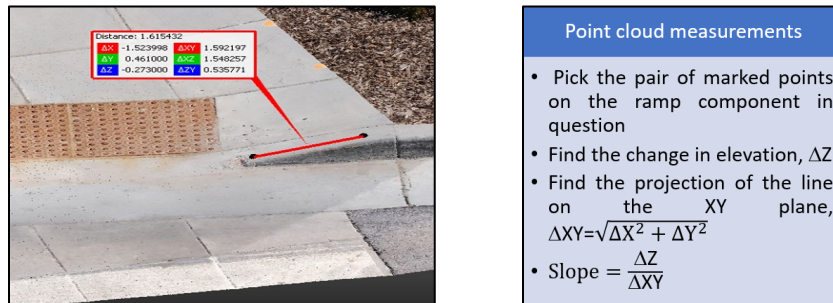
surface of the object of interest (e.g., the surface of the small and large traffic sign points in the point cloud models) to follow a standard measurement procedure as demonstrated in Figure 1.3.



**Figure 1.3** Linear accuracy evaluation

Cartesian distances of two ends of each side (edge) on the detected, usually rectangular, surfaces by k dimensional trees fusion are calculated as the length of that side. In this way, subjective measurements reduce considerably because selecting the endpoints of an edge in a point cloud can change to some extent operator by the operator. Because the superimposed facets on rectangular shapes in the point cloud (traffic signs, bridge surfaces, etc.) are not always a perfect rectangle, there might be some errors in this way of measurement. Nonetheless, this computed error is negligible.

The other metric for assessing the accuracy of the produced 3D models is the slope. To calculate the slope in the 3D space, we divide the rise line in the generated slope by the length of the run line in the same slope (triangle). Before that, we need to align the third axis of the point cloud model (the z-axis) with the elevation axis (the rise axis). That considered, the slope can be computed as it is illustrated in Figure 1.4.



**Figure 1.4** Slope measurement in created 3D models

Spatial data resolution in the generated point clouds lets us conduct the quality assessment of completeness. To do so, we calculated the number of points that are generated around each point within a certain radius in the point cloud model. The calculated value would give us the density distribution in the generated point cloud model.

Furthermore, the saturation metric of the point clouds is computed by calculating the total number of points with the same nearest neighbor distances. For an easier illustration of the results of these two metrics, histograms of both the density distribution and the saturation are made.



## 2. BACKGROUND

In this section, we review the literature regarding the applications of LiDAR and image-based 3D reconstruction technologies in the industry and research area. A brief description of each technology and how they work are also provided.

### 2.1 LiDAR Technology

The LiDAR technology is established in the engineering community and continuing to be used for several applications since it has been proven as a useful tool in a multitude of industries. In practice, there are three commercial types of laser scanners, as shown in Figure 2.1. These scanner types are time-of-flight (TOF) laser scanners, phase shift laser scanners, and triangulation-based laser scanners. Phase shift laser scanners are usually the fastest type of laser scanners. Nevertheless, their data-collection range is limited to approximately 80 meters around the sensor of the laser scanner when used for roadway scanning.



**Figure 2.1** Different types of laser scanners

The second type of laser scanner (triangulation-based scanner) can collect data in the range of a radius of fewer than five meters from the sensor of the laser scanner. Therefore, scanning small objects that are placed in the vicinity the laser scanner's sensor is conducive to their use. Most long-range scanning jobs are conducted by a time-of-flight LiDAR scanner since they have the highest range for data acquisition, thereby reaching up to 100s meters.

Nonetheless, the fact that this laser scanner can scan long-ranges results in a longer duration of the data acquisition and also, in many cases, lower accuracy compared to the other two laser scanner types. Time-of-flight laser scanners operate by emitting pulses of laser and receiving the same pulses that are reflected from the surface of an object. The returned pulse will be processed to calculate the characteristics of the scanned objects.

This laser scanner calculates the time of flight of the abovementioned pulse to compute the distance that is traveled by every single pulse. The differences in laser return times and changes in laser wavelengths are calculated together to build a virtual 3D representation of the scanned surface and its individual characteristics. Each one of the emitted pulses can save information, namely spatial coordinates, red-green-blue data, and density data.

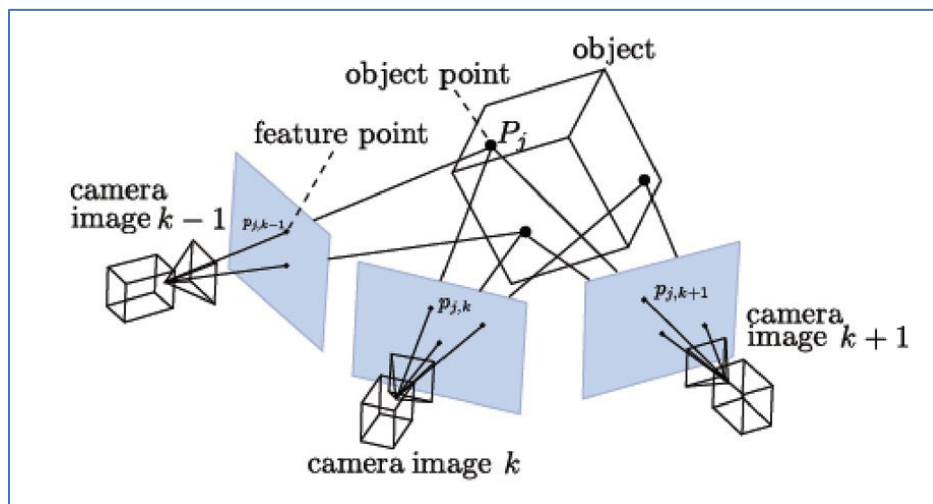
Over the course of scanning roadways, the spatial data will be organized and saved in the form of points that collectively build the overall point cloud model. Quite a few research studies have been conducted to assess the performance [9], accuracy [10], and quality of the laser scanners in reconstructing geospatial 3D data from different types of scenes [11] with various types of surfaces [12] and in different illumination conditions [13].

Even the old models of the LiDAR scanners offered a high-quality output (with errors in the order of less than one millimeter) at ranges from one and one-half meters to 50 meters in indoor settings, as described in reference number [10]. Moreover, some research on the reconstructed point cloud models of different surfaces demonstrate a slight decrease in accuracy of the laser-scanning technology while mapping dark surfaces. LiDAR technology has been employed for various transportation applications, including urban modeling, asset inventory, intersection modeling, asset encroachment collection, overhead clearance measurements of obstructions in the roadways, and the acquisition of pavement condition data.

## 2.2 Image-Based 3D Reconstruction Technology

Photogrammetric 3D reconstruction is the process of capturing 2D images from the 3D world and then, formatting the captured digital 2D images to build the 3D virtual models (point cloud models). In this approach, the 3D data of an object in the real world is captured by taking a set of images and/or digital video frames. The following summarizes the process of image-based 3D reconstruction, as it is also illustrated in Figure 2.2:

1. Image acquisition: In this step, at least two images are needed that include the point of interest in them (every single point in the real world to be reconstructed). Next, the captured images that contain the point of interest in the scene will go through the process of triangulation;
2. Feature extraction: The noticeable features in the digital images are points, such as corners that can be automatically detected to computationally characterize the digital images;
3. Camera calibration and image registration: This step of the photogrammetry intends to calculate the exact position of the camera while the associated digital image is captured. Particularly, it estimates the orientation of the cameras in the world coordinate. To that end, the recognized corner features in consecutive digital images are processed to calculate the intrinsic and extrinsic parameters of the associated digital camera;
4. Depth determination: In the last step of the structure from motion process (photogrammetric 3D reconstruction process), the corresponding points are found by matching the corner features between consecutive images to calculate the depth (spatial data) of the reconstructed points seen in the 2D images into the 3D virtual space by performing the triangulation process.



**Figure 2.2** Image-based 3D reconstruction; The Structure from Motion (SfM) technique

The feasibility of the image-based 3D reconstruction technique is investigated in the same way that is investigated for laser-scanning technology. The engineering applications that the image-based 3D reconstruction technology are tested for include transportation, construction, and structure-related applications [14].

Despite the lower precision of the photogrammetry technology in comparison to the laser-scanning technology [15], image-based 3D reconstruction of some civil infrastructure facilities [16, 17] and image-based progress monitoring of the construction projects are established methods for researchers working in the area of civil infrastructure engineering. Examples include the research conducted by Klein et al. [17]. In this research project, they worked on environmental limitations (e.g., occlusions of the objects of interest by the presence of labor, heavy construction equipment, and machinery, etc.) of image-based 3D reconstruction of facilities in the construction job sites. The other examples are as follows.

A line of research in this area relates to the science of videogrammetry. Videogrammetry is actually photogrammetry with only one difference. In the videogrammetry process, instead of digital static images, digital video frames (consecutive images captured during the recording time) are used in the process of structure from motion to build the series of features required for 3D reconstruction.

Nonetheless, because of the normally lower resolution of the recorded digital video frames in comparison to the taken static digital images, multiple research has been conducted that focuses on videogrammetry and quality of the video frames. In this direction, Pollefeys et al. [18] made use of digital video files to reconstruct 3D models of urban areas in a real-time fashion. Furthermore, Brilakis et al. [19] proposed an automated framework for data acquisition by use of the videogrammetry technique. Moreover, Rashidi et al. [20] presented a research paper proposing an optimization method for the selection of the keyframes within the recorded footage to make the most of the collected video data.

Among the existing research studies, there is a lack of study in determining the extent to which the photogrammetry technology can be used by transportation agencies for their tasks related to asset inventory. The motivation behind the current study relies on providing the transportation agencies with a study that determines the accuracy and quality of the photogrammetry technology when used for the associated applications with the task of asset inventory.

### **2.3 Automated 3D Modeling in Other Industries**

In other industries, such as the construction industry, there is a large number of research studies that prove that these automated sensing technologies can offer many advantages over conventional manual procedures. In this direction of research, Lato et al. [21] carried out a research study for mapping shotcrete thickness by leveraging LiDAR and photogrammetry as it is shown in Figure 2.3. Lato used this 3D data to correct the common over-calculations of shotcrete because of the convergence of the rockmass in the site.



**Figure 2.3** 3D modeling of constructed structures

In another research project, scientists realized that the use of LiDAR and photogrammetry technologies are vital for the preprocesses during the relocation of infrastructure facilities. For example, Veneziano et al. [22] investigated the need for accurate information about surface terrain during the construction phase. This information can be obtained readily by leveraging LiDAR and photogrammetry technologies. Veneziano et al. used laser scanning together with image-based mapping to accelerate the construction phases and save time and money.

Many of the aforementioned research studies found that both LiDAR and photogrammetry can be used together to perform engineering tasks in the real world. Furthermore, the correct and right usage of these technologies in different applications can cut costs and lost time in the projects. The speed and accuracy that these technologies can bring to engineering projects account for their initial upfront cost. That said, LiDAR and photogrammetry are on their way to becoming standard in the industry and engineering community.

### **3. METHODOLOGY**

Two main data collection procedures are tested according to the different possible data collection modes for various assets in transportation facilities. As for the roadway asset and pavement data collection, a mobile (vehicular) setting is used. This would allow a fast and automated setting for collecting transportation assets such as roadside traffic signs. The second procedure includes terrestrial scanning of the scene in a stationary setting. This would allow a better collection of data from facilities, such as pedestrian access ramps as a higher accuracy is required for inspection purposes.

#### **3.1 Mobile (Vehicular) Data Collection**

##### **3.1.1 Mobile LiDAR**

In this study, we used the mobile LiDAR data collected by Mandli Communication Inc. under their contract with the Utah Department of Transportation. Figure 3.1 elaborates upon their data collection setup. We obtained LiDAR models from connections within UDOT to carry out our comparisons between point clouds. We obtained a LiDAR model for each highway model that we generated using mobile photogrammetry (explained in the next subsection).

##### **3.1.2 Mobile Photogrammetry**

Data acquisition for the asset maintenance portion of this research project included evaluating a number of different camera settings, different speeds of the moving platform, illumination conditions, and directions of travel during the data collection procedure. At first, the city streets and routes were evaluated and considered for the data collection sessions. This helped us to find sections of the roadways with a smaller number of traveling cars (i.e., lower rate of occlusions) and also lower minimum speed limits (since at higher speeds there is a chance of losing visual information in the recorded video frames). This was done to evaluate the available 3D reconstruction software packages and their different parameters, and the hardware settings (digital cameras). This helped us fine-tune the data-collection procedure and prepare for the highway data collection that required us to drive at much higher speeds because of the traffic flow.

All of our mobile photogrammetric data collection sessions were conducted by a Toyota Tacoma and a suction cup mount (as it is displayed in Figure 3.2) to carry the digital camera. We used the GoPro series for the purpose of recording video footage of the roadways. We initiated the project by using an older version of the GoPro cameras (model GoPro Hero 3+ Black Edition). This camera could capture video frames with 4k resolution at the rate of 15 digital video frames per second and also 2.7k resolution was another option with a maximum rate of 30 digital video frames per second. However, the initial assessment of the reconstructed 3D models demonstrated that a higher rate of data capturing is needed when collecting data from highways.



**Figure 3.1** Mandli mobile LiDAR data collection setup (version X-35)

Due to the abovementioned reasons, we upgraded our digital camera and used a newer version of the GoPro series (GoPro Hero 8), which is an off-the-shelf and available digital camera. It is important to use affordable cameras to keep the data collection costs low since the motivation behind the project is to find an alternative solution to the existing expensive data collection methods. That said, we purchased the new digital camera to use as our photogrammetric sensor for the highway data collection sessions. The GoPro Hero 8 camera has a 12-megapixel sensor, the same as the older version of its series.

Nevertheless, the newer version excels over the older versions in terms of the video resolution and the rate of data capturing. The newer version of the GoPro camera could record video data with 4k resolution at 60 frames per second, 2.7k resolution at 120 frames per second, and 1080P resolution at 240 frames per second. The improved resolution and data capturing rate were vital for the purpose of the current research study.



**Figure 3.2** GoPro Mounted on a vehicle

Table 3.1 shows detailed information regarding the multitude of data collection sessions conducted to test the mobile photogrammetry setting. During the data collection sessions, we recorded the exact location of the road on the map, the direction that we were driving while collecting the video data, the camera video data setting (video resolution and the data capturing rate), the speed limit of the road, the speed that we were driving during the data collection procedure, the position of the camera on the car, the weather and illumination conditions, and the city/highway section.

It should be noted that we only documented the data collection sessions that were used for the process of 3D reconstruction, while the actual number of the data collection sessions are actually far more than the documented data listed in the following table.

The table demonstrates that the data collection sessions were critical in our research efforts. Once we successfully built acceptable 3D models of the city street roadways by using the new GoPro camera (GoPro Hero 8), we moved on to the next step of the data collection sessions for the asset management portion of the research, which was the highways. The fact that the minimum allowable traveling speed on highways is considerably higher than the minimum traveling speed on city routes and streets created some problems for the data collection crew. We could collect data at the speed of 25 miles per hour on the city streets. Nonetheless, the minimum traveling speed on highways ranged from 40 miles per hour to 60 miles per hour. It should also be noted that the traffic volume created a challenge for capturing the roadway assets while recording the video footage.

**Table 3.1** Mobile data collection details

Date & Time	Road Location	Direction	Recording Settings	Speed Limit	Actual Speed	Camera Position	Sky Conditions	Remarks
11/8/2020 1:00 PM	on 700W just off of 1700S	South	2.7K @ 30 fps	25	25	Centered	Sunny	City Street
11/18/2019 12:00PM	On 600W just off of 1700S	North	2.7k @ 30 fps	30	25	Centered	Sunny	City Street
1/14/2020, 12:45 PM	1300 S Between 900E	East	2.7K @ 30 FPS	30 MPH	25 MPH	Centered on hood	Sunny	City Street
2/08/2020, 1:45 PM	Driving North on 900W between 1700S and 1300S	North	2.7K @ 30 FPS	30 MPH	25 MPH	Centered on hood	Partly Cloudy with blue skies	City Street
2/11/2020, 2:00 PM	1300 S between 700E and 1100E	East	4K @ 30 FPS, Linear video mode	30 MPH	30 MPH	Centered on hood	Mostly cloud covered. Still good illumination	City Street
2/14/2020 1:00PM	I-15N	North	2.7k @ 120 FPS, Linear	70	60	centered on hood	Light cloud cover with good sunlight	Highway collection
2/17/2020, 2:00 PM	1301 S between 700E and 1100E	East	4K @ 30 FPS, Linear video mode	30 MPH	30 MPH	Centered on hood	Light cloud cover with good sunlight	City Street
2/19/2020, 2:00PM	I-15N	North	2.7K @ 120 wide	65	60	centered on hood	No clouds. Sunny	Highway collection
2/19/2020, 2:00PM	I-215N	West	1080P @ 120 Linear	65	60	centered	No clouds. Sunny	Highway collection
2/20/2020, 11:00 AM	I-15N	North	2.7k @ 60 FPS, Linear	65	~60	Centered	Light cloud cover with good sunlight	Highway collection
2/20/2020, 11:00 AM	I-15N	North	4k @ 60 Wide	65	60	centered	No clouds. Sunny	Highway collection
2/21/2020, 2:00 PM	I-201 East	East	2.7K @ 60 linear	65	60-65	one view left, one center, one right	No clouds. Sunny	Highway collection
2/23/2020, 3:00 PM	I-15N	North	4K @ 30 FPS, Linear video mode	65	55	one view left, one center, one right	Very little clouds	Highway collection
3/15/2020, 9:45 AM	I-15N	North	1 run with 4K @ 60 fps and 2 runs with 2.7K @ 120 fps	65	45-55	Centered View	Very little clouds	Highway collection
3/15/2020, 11 AM	I-15N	North	2.7k @ 120 FPS wide	65	55-60	Centered	No clouds	Highway collection
3/23/3030, 10:45:00 AM	I-15N	North	2.7K @ 120 FPS wide	65	55	centered	Cloudy, storm moving in, low sunlight	Highway collection

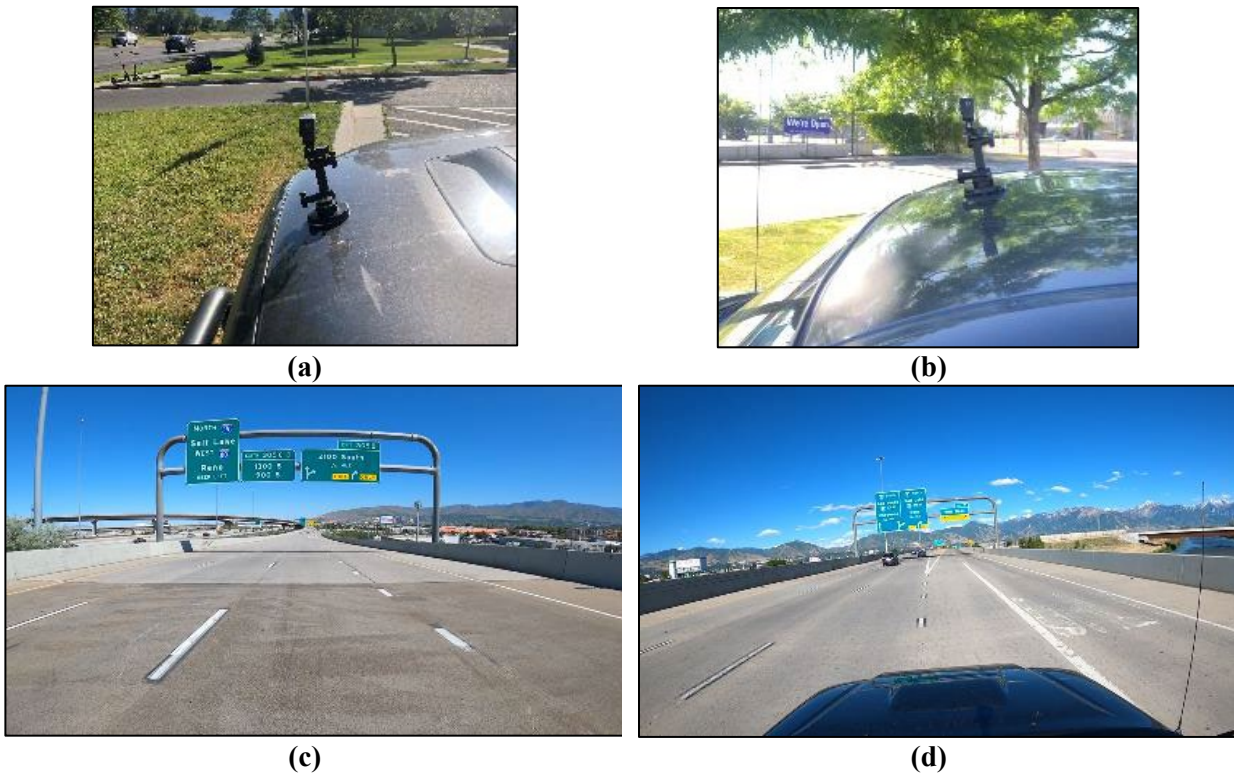


Date & Time	Road Location	Direction	Recording Settings	Speed Limit	Actual Speed	Camera Position	Sky Conditions	Remarks
3/24/2020, 11:00 AM	I-15N Exit	North then South	2.7K @ 120 Wide	25 MPH	20 MPH	Centered	Cloudy, low sunlight	Highway collection
4/28/2019 5:30 PM	I-80E	East	2.7K @ 120 Wide	65	50 MPH	Centered	No clouds	Highway collection
5/9/2020 11:00 AM	Driving north on I-15	North	4k@60wide 4k@60linear 2.7K @ 60 linear 2.7K @ 120 wide 1080 @ 240 Wide 1080 @ 120 Linear	60	45-50	Centered	No clouds	Highway collection
5/17/2020 2:00PM	Driving North and south on I-15, driving east on I-80	North, South, East	2.7k @ 120 wide	65-70	50-55	Centered	Cloud coverage, low sunlight	Highway collection

Similar to our experiments conducted for the city streets, our experiments for highways included testing all possible variations of video resolutions and the data capturing rate (by using the new version of the purchased digital camera). These experiments helped us find the optimum solution for the data collection procedures for the highway setting.

Among the tested combinations that we tried in highway settings, the best point cloud model was the result of the video capturing data with a resolution of 2.7k pixels, which was collected at the rate of 120 digital video frames per second. We used both wide and linear field of views in our experiments. Some of the field of views built into the camera were limited to a small portion of the front view, thereby resulting in losing visual information of the side highway features (e.g., traffic signs).

After evaluating the resolution and frame rate combinations, we experimented with different settings regarding the angles and heights of the camera mounts. We decided to test whether mounting the camera on the hood of the vehicle or on the roof of the vehicle would work better for data collection. After testing both of the mentioned settings, based on the produced data in the two cases, we concluded that a camera mounted on the hood is a better setting compared to a camera mounted on the roof of a vehicle. As it is demonstrated in Figure 3.3 b, when the camera is mounted on the car roof, it is difficult to avoid the car hood in the field of view of the cameras. The reflecting car hood caused problems in the process of image registration as the software had difficulty in pairing the images due to a fixed image feature (the corners detected in the image of the car hood) in almost all of the images (Figure 3.3 d).



**Figure 3.3** Different mounting areas and the corresponding view on the bottom

A hood-mounted camera was easy to orient in a way such that the whole roadway scene and all traffic signs are in the field of view, all while avoiding the parts of the vehicle (such as the front hood area) from the video, as it is shown in Figure 3.3 a and Figure 3.3 c.

## 3.2 Terrestrial Data Collection

### 3.2.1 Terrestrial LiDAR

Our data collection crew used a Maptek I-Site 8820 terrestrial laser scanner (as shown in Figure 3.4) to conduct the terrestrial LiDAR portion of this case study. This terrestrial scanner is a long-range laser scanner that can send pulses to distances of up to 2,000 meters. The LiDAR scanner also has the capability of built-in panoramic imaging to produce accurate point cloud models with red-green-blue (RGB) color representation.



**Figure 3.4** Maptek I-Site 8820 terrestrial LiDAR

The Maptek 8820 LiDAR gives the user the opportunity to customize the settings using a Panasonic tablet. This tablet also lets the user preview the scanning area based on the parameters that he/she set for the lighting conditions, point cloud density, image capture, and necessary accuracy. Once the parameters are set, the rest of the procedure is completed automatically by the laser scanner. Since the laser scanner rotates at a high rotational speed during the scanning time, a sturdy tripod should hold the body of the laser scanner.

### **3.2.2 Terrestrial Photogrammetry**

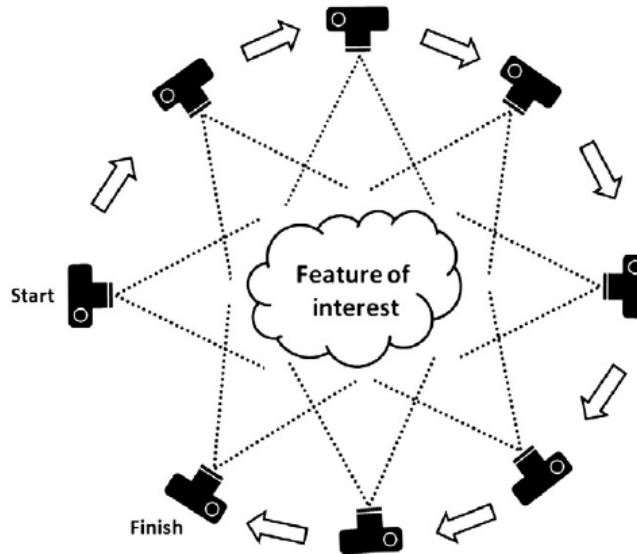
A terrestrial photogrammetry setup is used for the collection of pedestrian access ramp spatial data. To that end, the data collection crew took digital images using a digital camera in a semi-static procedure to capture images from each point of the scene at least twice. We used a Fujifilm XT-30 mirrorless digital camera (as it is demonstrated in Figure 3.5) for this part of the project. The Fujifilm XT-30 has a large 26.1 MP sensor capable of capturing high-quality images with enough pixel information in each image for an inspection job that requires a high level of accuracy (in the order of millimeters).

To perform the data collection procedure in this project, each one of the pedestrian access ramps is considered as a center of a hypothetical circle and we moved along the perimeter of that circle, having the digital camera oriented toward the center of this circle while taking consecutive images of the scene. This procedure permits having a sufficient number of pairing points in the pair of images. It is critical to stay far enough from the center point of the circle (access ramp) to record all pertinent components of the pedestrian access ramp, but not too far, making it difficult for the camera to collect enough detail on all components.



**Figure 3.5** Fujifilm XT-30 mirrorless digital camera

The moving pattern around the object of interest (pedestrian access ramp) is depicted in Figure 3.6. This pattern of image data collection allows us to have enough overlap image content between all digital images, which is necessary for a successful alignment of the images by the 3D reconstruction software packages. On average, we built each pedestrian access ramp model by using 30 digital images. It is noteworthy to mention that too many images may result in a very high density of the point cloud models, thereby increasing the file sizes and reducing the speed of the software package for image registration and 3D reconstruction.



**Figure 3.6** Circular pattern for image acquisition

Table 3.2 tabulated the image-based and LiDAR-based data collection details for collecting the spatial data of the pedestrian access ramps. We recorded the number of models at each location, the acquisition time, the exact number of images taken per ramp, the software processing time for 3D reconstruction, the total number of points in the 3D point cloud model, and the file sizes. It is important to ensure that all procedures are conducted in a way such that file sizes are optimal for processing and transferring between transportation agencies.

Table 3.2 Terrestrial data collection details

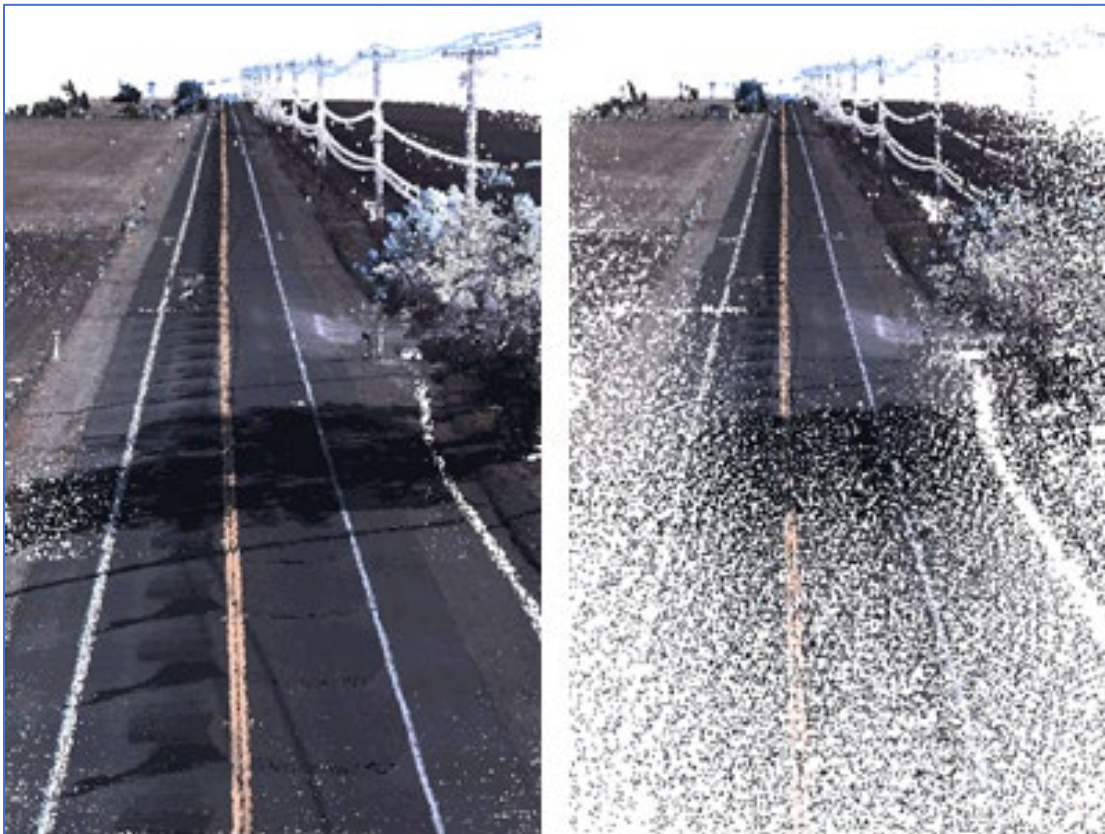
<b>Method</b>	<b>Model</b>	<b>Acquisition Time (Minutes)</b>	<b>Number of images/scans (Aligned/Total)</b>	<b>Processing Time</b>	<b>Number of Points in Point Cloud</b>	<b>File Size (GB)</b>
Image-Based Reconstruction	Ramp 1	< 5 min	31/31	47 min 2 sec	258,651,814	6.72
	Ramp 2	< 5 min	37/37	52 min 22 sec	429,797,343	11.17
	Ramp 3	< 5 min	27/29	52 min 26 sec	313,767,481	8.16
	Ramp 4	< 5 min	31/31	47 min 8 sec	263,338,208	6.87
	Ramp 5	< 5 min	27/29	51 min 23 sec	436,552,997	11.35
	Ramp 6	< 5 min	24/25	49 min 20 sec	247,958,617	6.45
LiDAR-Based Reconstruction	Ramp 1	16 m 30 s	1 scan	NA	12,182,400	768
	Ramp 2	17 min	1 scan	NA	11,955,200	745
	Ramp 3	12 m 9 s	1 scan	NA	3,498,634	222
	Ramp 4	13 m 45 s	1 scan	NA	6,506,448	407
	Ramp 5	13 m 9 s	1 scan	NA	2,999,779	102
	Ramp 6	13 m 32 s	1 scan	NA	2,398,708	83

## 4. ASSESSMENT METRICS

### 4.1 Quality and Accuracy Metrics for Mobile Procedures

Regarding the quality and accuracy assessment of the created models, we compared the 3D models using photogrammetry and the created models using LiDAR technology. As is shown in Figure 4.1, we first assessed the quality of the created models by comparing their overall density using density algorithms, including the number of neighbors. To calculate the number of neighbors for each 3D model, we first needed to target each one of the points one by one and then numerate the total number of the generated points in the neighborhood of the associated target point. To do so, the software defines a radius of a sphere and then enumerates the number of points within a sphere with that radius.

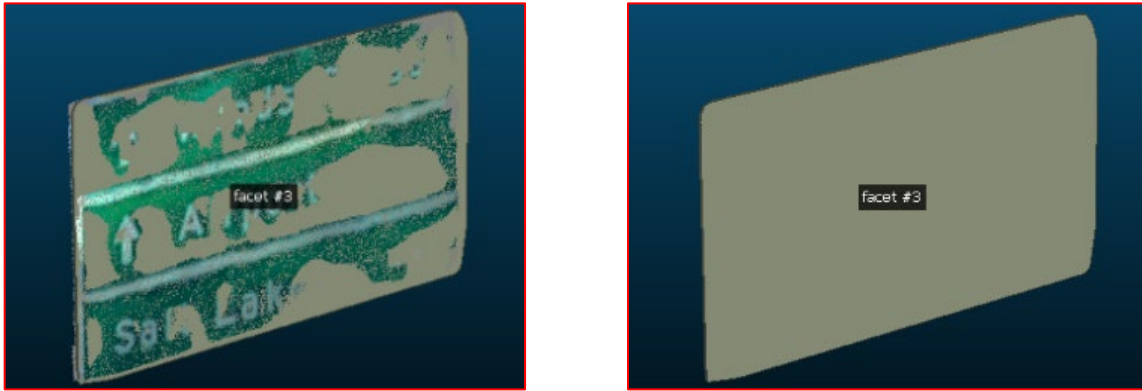
These spheres were superimposed on the entire point cloud to achieve an overall index of uniformity. We used an equivalent radius of one centimeter, meaning that the size of the radius of the defined sphere is one centimeter in the real world. We used the equivalent radius because both the photogrammetry model and LiDAR model are in arbitrary units once reconstructed by software packages.



**Figure 4.1** Dense point cloud model vs sparse point cloud model

To calculate the equivalent radius in the real world, we extracted some of the measurements in both the real-world scene and the created point cloud model. By comparing the distances in the two abovementioned spaces, we computed the one-centimeter equivalent radius in the 3D point cloud model. Using the equivalent radius, we calculated the histograms and point cloud saturation images as well for better visualization of the density of the 3D models.

We also evaluated the accuracy of the reconstructed traffic signs and other elements of the highways. In doing so, we compared the ratios of height to width in the generated planar objects with the actual ratios of height to width in the real world. Therefore, we measured the aforementioned ratio for the planar objects generated in the photogrammetric and LiDAR-based 3D models as well as the actual ratios measured in the scene or by using the actual size (standard size) of those planar objects (e.g., traffic signs in the side of the highways).

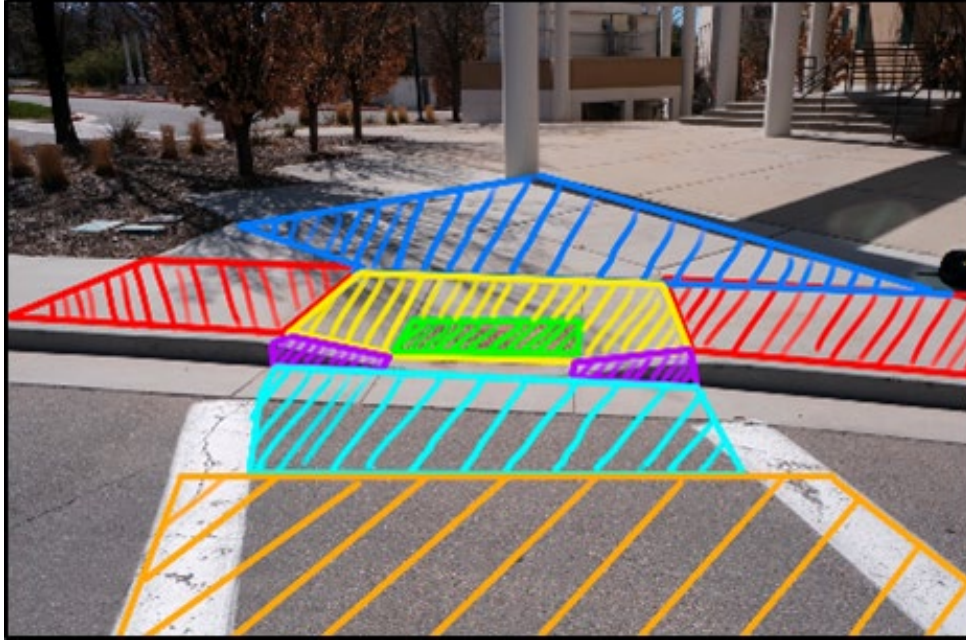


**Figure 4.2** Super imposed facets for measurements of the traffic sign edges

## 4.2 Quality and Accuracy Metrics for Terrestrial Procedures

We collected several pedestrian access ramps, and each one of them was located in different parts of Salt Lake City, allowing us to have well-distributed data in terms of the variety of the pedestrian access ramps and their design. To conduct the data collection sessions for the pedestrian access ramps, we first needed to understand the standard procedures that transportation agencies are currently doing for inspecting these ramps. Therefore, we met with the Utah Department of Transportation engineers and documented the inspection procedure of the different components of the pedestrian access ramps.

The standard procedure for inspection of the pedestrian access ramps is also outlined in the UDOT C-170 Pedestrian Access Ramp Evaluation form. However, our meeting with the engineers from the Utah Department of Transportation was necessary since there are quite a few components of the pedestrian access ramp, as it is shown in Figure 4.3, and each one of the components has its own specific measurement requirement.



**Figure 4.3** Pedestrian Access Ramp Components. Red: Pedestrian Access Route (PAR), Blue: Turning Space (T), Yellow: Ramp, Purple: Flares, Green: Detectable Warning Surface (DWS), Light Blue: Clear Space, Orange: Crosswalk

The engineers from the Utah Department of Transportation used a Smart Tool Smart Level (as it is shown in Figure 4.4) and a tape measurer to conduct the inspection of the pedestrian access ramps. The former was used to calculate the slope of each one of the ramp components in percentages. The percentages should be in the predefined tolerances for the ramp to be considered a standard ramp. Also, the width and length of each component should be in a certain range, which is inspected by using the tape measure.

Upon completion of the inspection procedures with the representatives (engineers) of the Utah Department of Transportation, we kept the inspection reports from each target pedestrian access ramp inspection. Therefore, we used the measured components by the engineers in the reports as the ground truth measurements to compare them with our virtually collected measurements from the 3D point cloud models of the pedestrian access ramps.

We evaluated the 3D models of the pedestrian access ramp quality in the same way as we did the asset management part of the project. Therefore, we calculated the density of the 3D point cloud models using an equivalent length in the actual scene and calculated the total number of neighbors for each point of the point cloud.

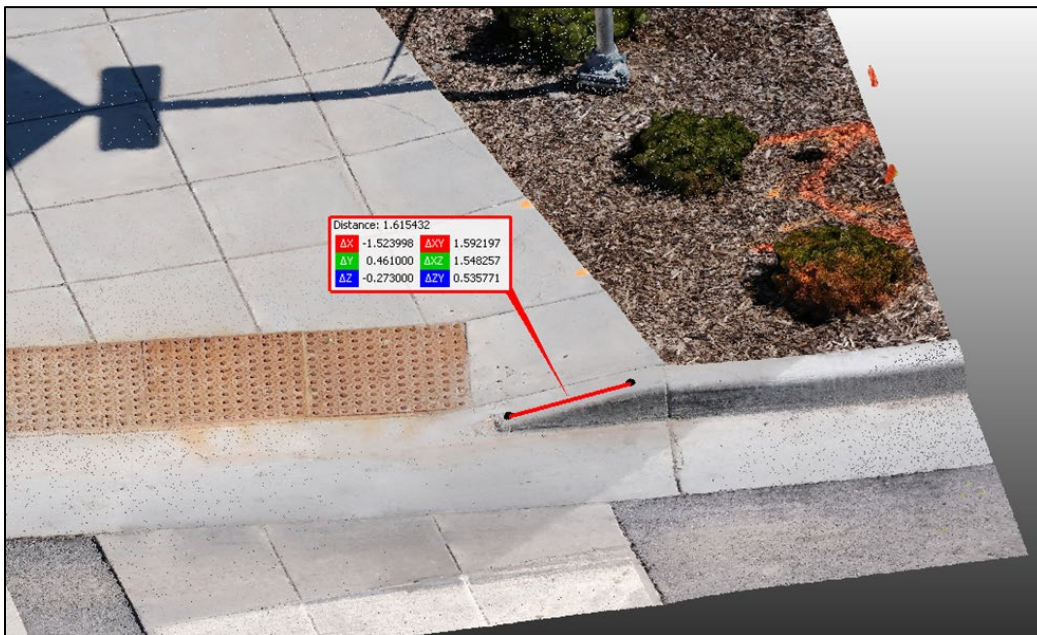
Another important measurement recorded from access ramp inspections is the slopes of various components of the pedestrian access ramps. To increase the accuracy of the measurements, each component of the pedestrian access ramp is calculated at least three times, and the average number is considered as the finalized measurement for that component.





**Figure 4.4** Smart Tool Smart level

Each component of the pedestrian access ramp has different slope and distance tolerances based on the guideline for accessibility of the facilities issued by the Department of Transportation. To measure the slopes in the 3D virtual space, we first aligned the z-axis of the model to the elevation axis and then the slopes can be measured as follows. We first pick the two ends of a line whose slope is of interest and then calculate the slope based on the formula depicted in Figure 4.5 (by dividing the change in the Z coordinate by the distance of the projected line on the XY plane).



**Figure 4.5** Slope measurement of a flare component of a pedestrian access ramp.  $\Delta Z$  is the change in elevation,  $\Delta XY$  is the projected distance along the XY plane.

Furthermore, we evaluated the quality and accuracy of the reconstructed bridge models. In doing so, we measured the beam elements of the bridges that are reconstructed by mobile photogrammetry and the stationary-terrestrial LiDAR model. For this specific case, the LiDAR models provided by Mandli Communication Inc. did not contain the complete model of the bridges (e.g., the beam elements).

The pavement portion of the project was evaluated by detailed measurements of the cracks in the target pavement (a pavement area on the campus of the University of Utah). By laying the LiDAR data over the mobile photogrammetry data, we measured the extent to which the mobile photogrammetry can map the pavement information. For this specific experiment, we did not have the mobile LiDAR data and had to use terrestrial LiDAR, which gives more accurate data that can be used as the ground truth for evaluating the mobile photogrammetric 3D models.

## 5. RESULTS

Data evaluation of the reconstructed roadway point clouds is important to understand whether or not photogrammetry technology would give enough data to be comparable to the LiDAR technology procedures. This section evaluates this matter by 3D data analyzing as described in Section 4.

### 5.1 Software Packages Comparison

There are a large number of software packages that can be utilized for image-based 3D reconstruction. Nevertheless, most of them are designed for semi-static or drone data collection in which the sensor record data in a circular pattern around the object of interest. For the asset management portion of this project, we needed to find the best software package that would work for our case because of the linear nature of data acquisitions. This was conducted by leveraging a control set of 163 images that were taken during data collection of city street routes, as tabulated in Table 5.1.

The exact same 163 digital images were uploaded into each software package, and variables, such as registered images, processing time, number of points, and overall point cloud quality, were assessed. It is critical to select software packages that yield a dense enough point cloud output and clear enough spatial data. After assessing the data output from each software package, we chose Context Capture and 3DF Zephyr for the asset management portion of our research since they provided the most comprehensive and complete 3D models. Based on the final results and the quality of the point cloud models, we used Context Capture for photogrammetric 3D reconstruction purposes in our tests.

**Table 5.1** Comparison of different software packages using a control set of 163 images

Software Package	# Registered Images (of 163)	Processing Time (hrs)	Number of Generated Points	Point Cloud Quality
Agisoft	89	3.5	21 million	Not Good
Reality Capture	161	3	12 million	Not Good
3DF Zephyr	163	2	2 million	Good
Context Capture	163	1.75	55 million	Great
Pix 4D	163	4	1 million	Not Good

### 5.2 Results of the Mobile Collected 3D Data

#### 5.2.1 Roadway Assets (Traffic Signs)

Overall, the produced photogrammetry 3D point cloud models were comparable to the provided LiDAR 3D point cloud models (from Mandli Communication) in terms of density and accuracy. One important factor to mention is the densities of point clouds generated by photogrammetry and point clouds generated by LiDAR. In each case, the density of the photogrammetry point cloud model is much higher than the LiDAR point cloud models. Even though LiDAR tends to produce a denser point cloud compared to photogrammetry in the same settings, because of the mobile nature of data collections, the LiDAR point cloud models were not as dense as they are in the terrestrial settings.

Another factor was the number of frames per second used to extract frames from digital video data. We evaluated quite a few different frames per second settings, including 100, 90, and 50 frames per second. We chose 50 frames per second for most of our models because this number of frames per second was an optimum number for making the file size small and, at the same time, having visible models with sufficient density. We evaluated six different segments of highway roadways to evaluate the quality and accuracy in the creation of the traffic signs (e.g., overhead and roadside signs). Table 5.2 demonstrates the details regarding the Context Capture photogrammetry settings to build the image-based 3D point cloud models.

**Table 5.2** Data collection and processing for asset management models

Model	Lighting Conditions	Traveling Speed (MPH)	Len (Miles)	Number of Registered Images (Aligned/Total)	Processing Time (Image-Based)	Number of Points
Model 1	Dense Clouds, Intermittent light	50	0.25	999/999	2 hr 11 min	410 Million
Model 2	Sunny, perfect sign visibility, no reflections	45	0.25	1195/1195	2 hr 48 min	430 Million
Model 3	Sunny, perfect sign visibility, no reflections	20 (Exit)	0.1	1026/1026	2 hr 58 min	771 Million
Model 4	Bright sunlight, many reflections	45	0.5	850/850	2 hr 5 min	776 Million
Model 5	Indirect sunlight, low light on signs	45	0.25	850/850	2 hr 41 min	706 Million
Model 6	Sunny, good sign visibility	40	0.2	1107/1301	3 hr 42 min	1.3 Billion

Table 5.3 tabulated complete and detailed information of all sign ratios (height to width) calculated from the image-based and LiDAR-based point cloud models. Traffic signs were divided into small, medium, and large traffic sign groups. The overall accuracy of the reconstruction of all signs was also computed. The overall relative error of the photogrammetric point cloud models was within 1% of the relative errors calculated in the LiDAR point cloud models.









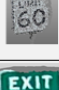

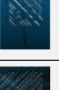




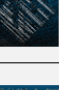
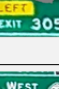
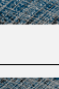
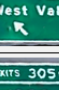
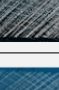


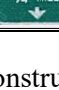

We used the standard deviation and coefficient of variation (CV) for each point cloud to find the well-distributed point cloud models in terms of density. A high value of the coefficient of variation means that the point cloud has less uniform spatial data. As it is shown in Table 5.3, the LiDAR point cloud models have a lower value of CV. It means that the LiDAR point cloud models are slightly more uniform than the photogrammetric point cloud models. The visibility of the traffic signs is another important factor for virtual inspection purposes. In photogrammetry 3D models, large traffic signs, such as overhead signs, can be easily read. As the traffic signs get smaller in size, their readability is reduced. Nevertheless, they still provide geometric data. Also, traffic sign ratios can be calculated from spatial data. Traffic signs, such as mile marker signs and speed limit signs, are slightly hard to read, but their sign ratios can still be calculated to measure the linear accuracy of the 3D reconstruction methods.

**Table 5.3** Measurement overview of image-based and LiDAR-based point clouds for asset management

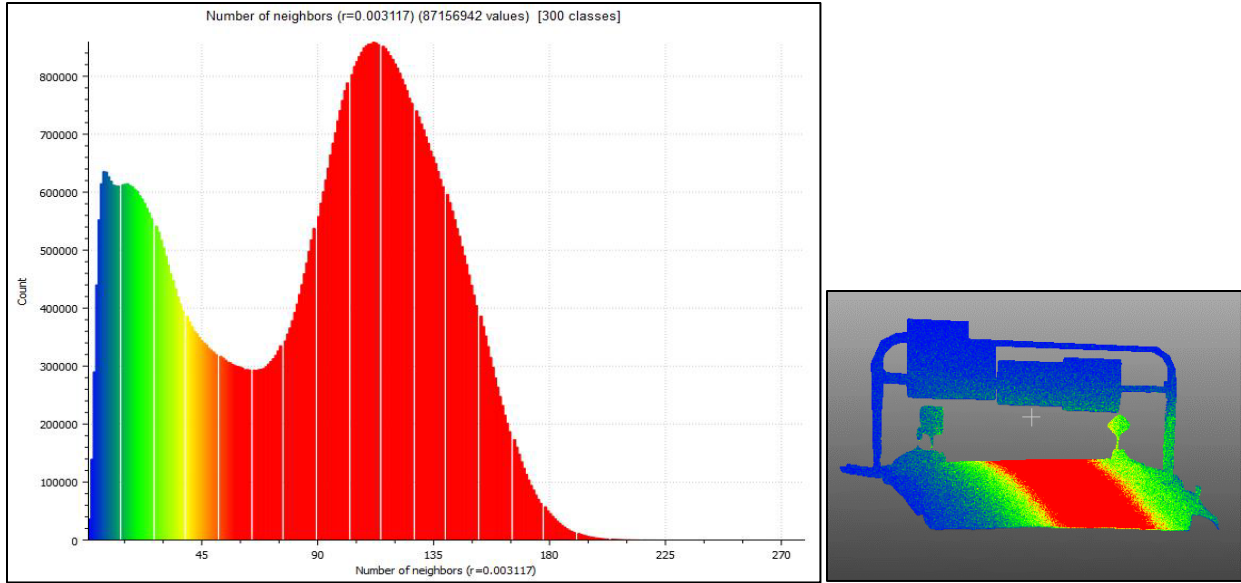
Model	Sensing Technology	Sign Ratio Errors (%)			Overall Model Error (%)	Average Sign Density (Points/in <sup>2</sup> )	Standard Deviation of Sign Density	Coefficient of Variation (CV)
		Small	Medium	Large				
Model 1	Image-Based	2.11	6.89	4.70	5.09	35.3	18.4	0.52
	LiDAR	4.39	5.40	1.51	3.93	0.74	0.32	0.44
Model 2	Image-Based	1.68	7.40	6.42	5.35	14.7	5.38	0.37
	LiDAR	2.78	1.56	6.41	3.81	0.89	0.37	0.42
Model 3	Image-Based	5.90	4.69	6.96	5.16	35.4	13.1	0.37
	LiDAR	2.96	2.91	4.25	3.48	0.96	0.41	0.42
Model 4	Image-Based	3.61	2.56	5.92	3.94	21.9	12.2	0.56
	LiDAR	1.71	2.15	4.93	2.81	0.61	0.20	0.33
Model 5	Image-Based	3.61	2.56	5.92	3.51	38.8	24.8	0.64
	LiDAR	1.71	2.15	4.93	2.73	0.91	0.47	0.52
Model 6	Image-Based	1.22	4.45	3.29	2.92	28.0	13.7	0.49
	LiDAR	1.23	3.27	3.47	4.11	1.63	0.67	0.41
Averages	<b>Image-Based</b>				<b>4.33</b>	<b>29.0</b>	<b>14.6</b>	<b>0.49</b>
	<b>LiDAR</b>				<b>3.48</b>	<b>0.96</b>	<b>0.41</b>	<b>0.42</b>

After assessing the six generated 3D models, traffic signs and pavement marking were reconstructed near to reality. In places where the bridges cast a dark shadow on the road, the illumination changes dramatically while driving under the deck of the bridge. This sudden change in the illumination caused a slight break in the reconstructed models of the bridge. Table 5.4 tabulated the sample images of the reconstructed traffic signs, the measurements regarding the ratio of height to width of the planar objects, the actual image of the traffic signs, and the surface density of the virtual traffic signs. Other than the singular mile marker sign, all other traffic signs were generated in a visible condition, and most relative errors (calculated by measuring the ratios of height to width) are notably low.

**Table 5.4 Model 1 Traffic Sign Details**

Sign Size	Image-Based Measurements									LiDAR-Based Measurements						
	Image from model	Height	Width	Ratio (H/W)	Sign Density (Points/in <sup>2</sup> )	Image of actual sign	Sign Code (MUTCD)	Actual Ratio (H/W)	Percent Error	Image	Height	Width	Ratio (H/W)	Sign Density (Points/in <sup>2</sup> )	Actual Ratio (H/W)	Percent Error
Small		0.3	0.1	3	37.28		D10-A	3	1.48E-14		0.96	0.34	2.82	0.69	3.00	5.88
Small		Sign not fully generated	Sign not fully generated	Sign not fully generated	Sign not fully generated		Sign not fully generated	Sign not fully generated	Sign not fully generated		0.93	0.31	3.00	0.97	3.00	0.00
Small		0.25	0.087	2.87	31.37		D10-A	3	4.21		0.89	0.32	2.78	0.40	3.00	7.29
Medium		0.5	0.38	1.32	56.02		R2-1	1.25	5.26		1.51	1.19	1.27	0.68	1.25	1.51
Medium		0.53	0.4	1.33	30.89		E5-1C	1.5	11.67		2.06	1.44	1.43	0.47	1.50	4.63
Medium		0.41	0.41	1.00	73.16		W4-2R	1	0.00		1.65	1.53	1.08	0.96	1.00	7.84
Medium		0.45	1.13	0.40	13.28		E1-5BP	0.36	10.62		1.41	3.64	0.39	0.34	0.36	7.60
Large		1.08	1.7	0.64	22.68	Sign Varies	E6-2A	0.68	6.09		3.62	5.48	0.66	0.50	0.68	2.35
Large		0.86	1.26	0.68	28.47	Sign Varies	E6-2A	0.6667	2.38		2.92	4.35	0.67	1.02	0.67	0.69
Large		1.03	1.06	0.97	24.55	Sign Varies	E6-2A	0.92	5.62		3.52	3.77	0.93	1.33	0.92	1.49

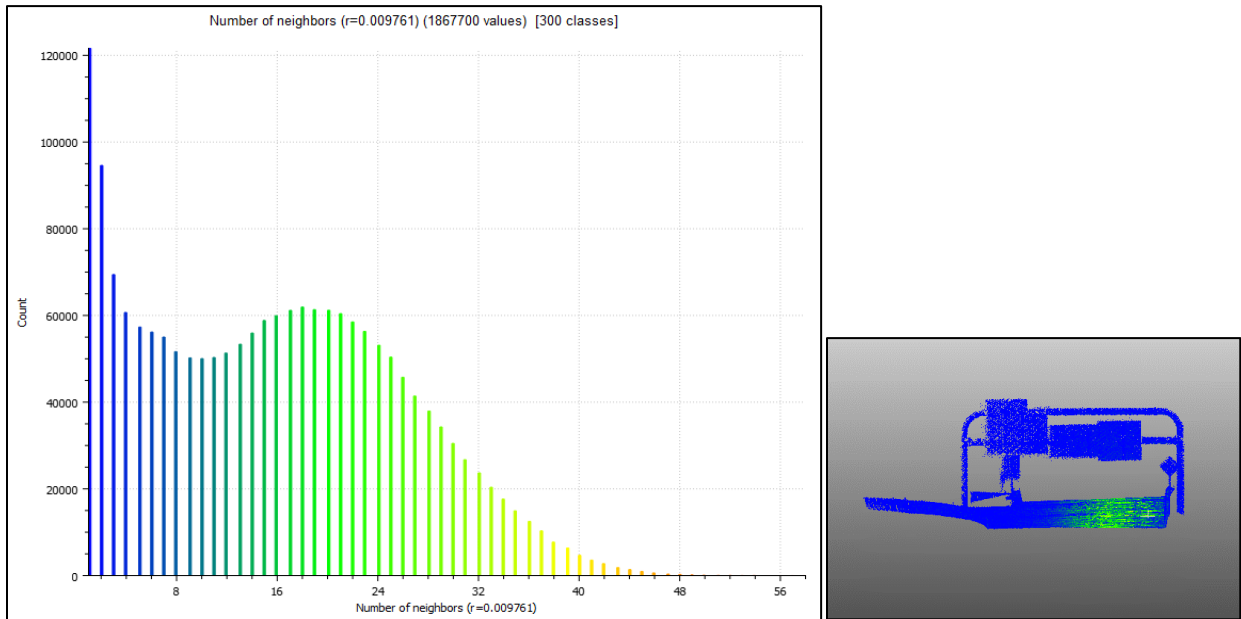
The reconstructed photogrammetry models were generally denser than the reconstructed LiDAR-based models. One important factor that can be seen in Figures 5.1—5.6 is the saturation of generated points in the model. Both models have higher saturation near the sensors. As generated points get farther from the sensor, they become less dense.



(a)

(b)

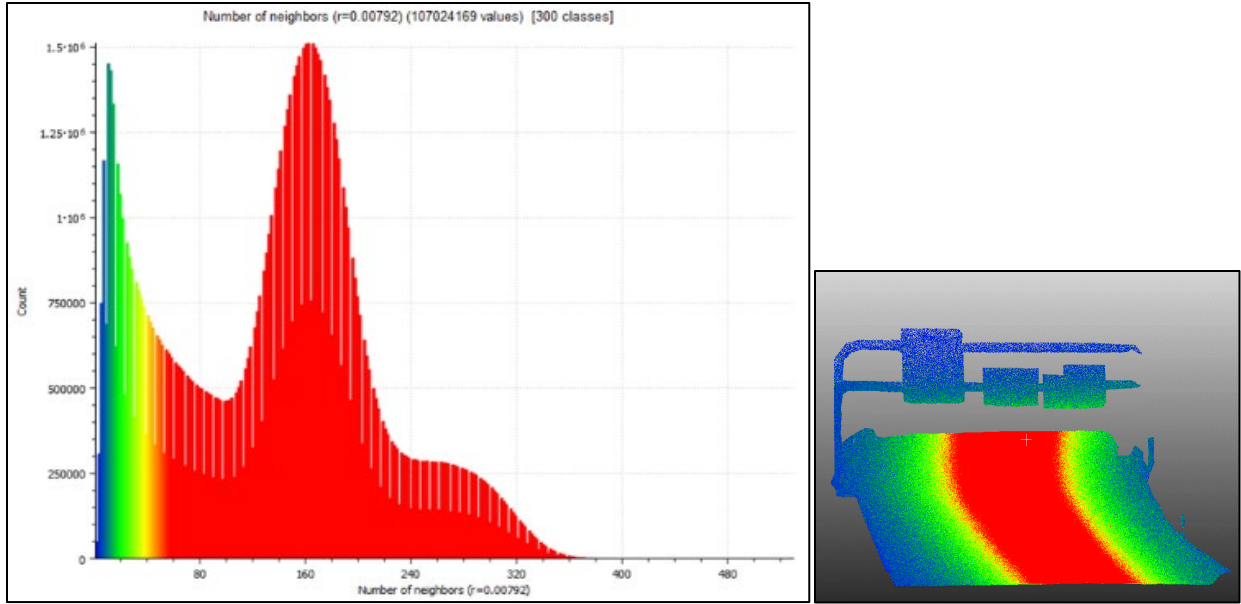
**Figure 5.1** The photogrammetric point cloud for model 1; (a) Density histogram (number of neighbors); (b) Model Saturation (red: the most saturated part, blue: the lowest saturated part)



(a)

(b)

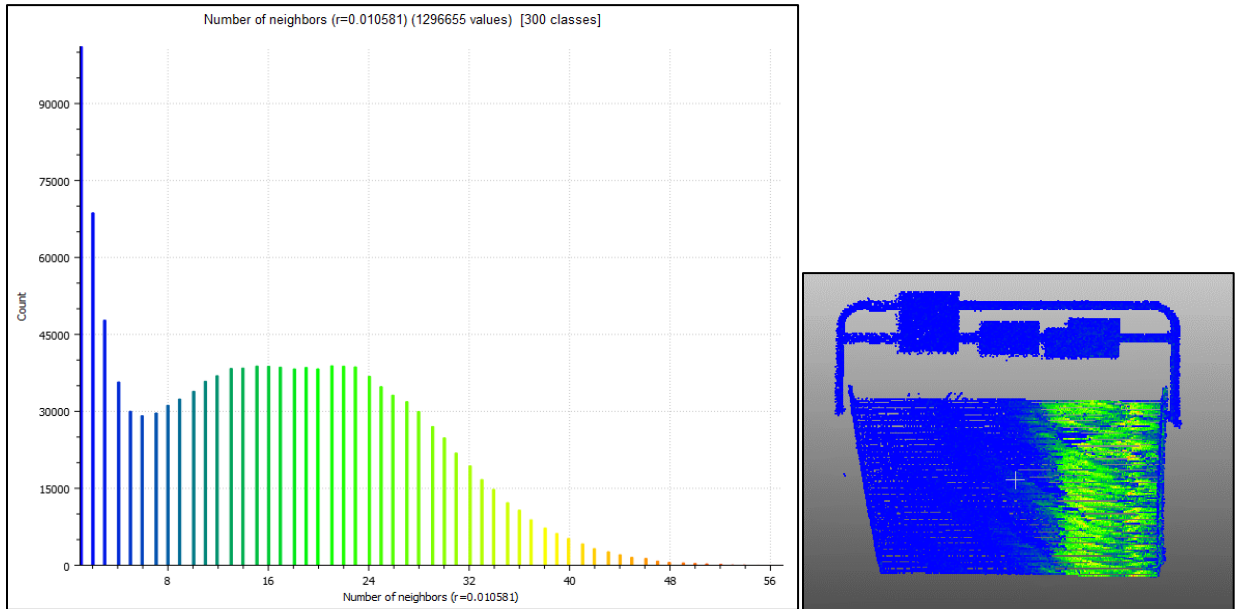
**Figure 5.2** The LiDAR point cloud for model 1; (a) Density histogram (number of neighbors); (b) Model Saturation (red: the most saturated part, blue: the lowest saturated part)



(a)

(b)

**Figure 5.3** The photogrammetric point cloud for model 2; (a) Density histogram (number of neighbors); (b) Model Saturation (red: the most saturated part, blue: the lowest saturated part)

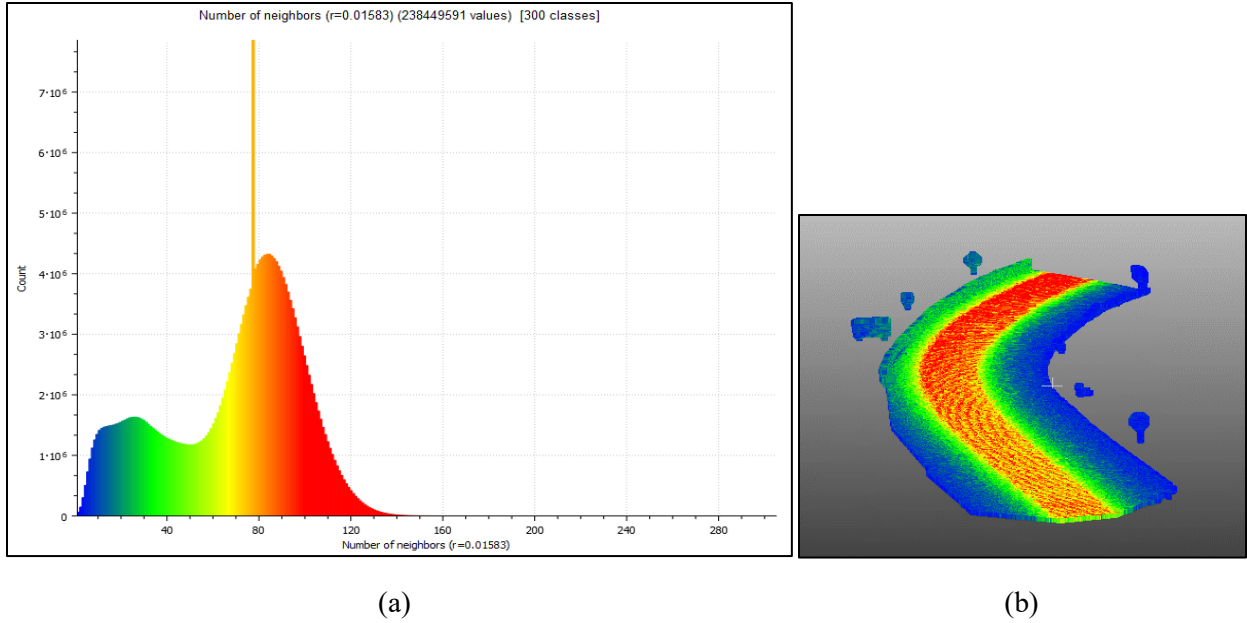


(a)

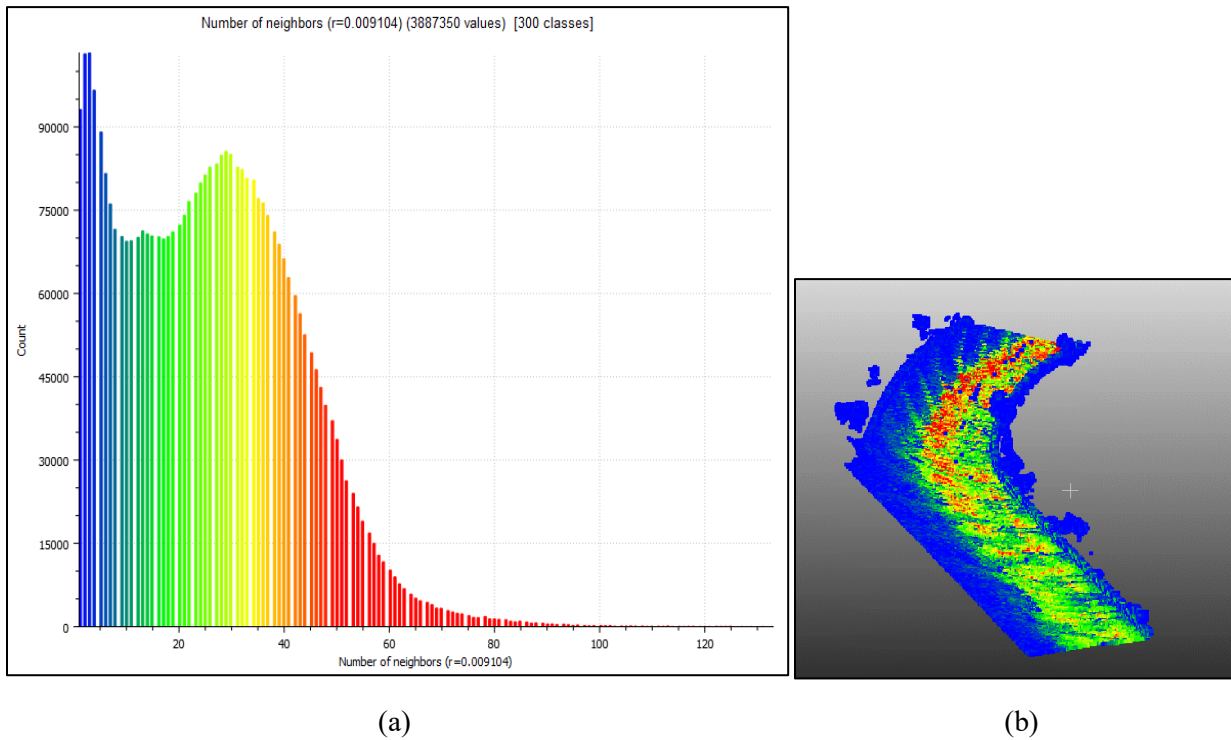
(b)

**Figure 5.4** The LiDAR point cloud for model 2; (a) Density histogram (number of neighbors); (b) Model Saturation (red: the most saturated part, blue: the lowest saturated part)





**Figure 5.5** The photogrammetric point cloud for model 3; (a) Density histogram (number of neighbors); (b) Model Saturation (red: the most saturated part, blue: the lowest saturated part)



**Figure 5.6** The LiDAR point cloud for model 3; (a) Density histogram (number of neighbors); (b) Model Saturation (red: the most saturated part, blue: the lowest saturated part)

The densest section of all three sections is the part named model 3, and this is because that section three is located in an exit roundabout off of the highway. Therefore, the data collection crew was traveling at a much slower speed as opposed to highway traveling speeds for sections one and two. This fact holds true for the LiDAR model, too. The laser-scanning model for this particular section is denser than other

LiDAR models. This illustrates that the slower we travel, the more detailed data the sensors can gather. Also, the accuracy of the generated models increases. The overall error of the photogrammetric models for this section is less than 6%, and it is still comparable to the LiDAR point cloud models.

To measure the size of the traffic signs (the actual sizes), we used the Utah Standard Highway Sign Supplement, The Manual on Uniform Traffic Control Devices (MUTCD), and UDOT's publicly shared highway sign map overlay. The sign codes are also provided by the Manual on Uniform Traffic Control Devices and UDOT's highway sign map to help the reader have a definite understanding of the exact sign.

## 5.2.2 Pavement

The objective of this case study was to assess the feasibility of close-range photogrammetry in the documentation of pavement distresses while reconstructing the 3D models of the roadways using a slow-speed version of mobile photogrammetry. We performed this field test in an area with no traffic to avoid having other vehicles' occlusion when we used the terrestrial LiDAR. The job site was in a parking area on the University of Utah campus area, and the data was collected on a sunny day.

For this experiment, we used the highest possible quality of the video-capturing setting using our GoPro Hero 8 camera because pavement distresses are usually much smaller than traffic signs. Therefore, we had video resolution set to 4k linear mode to avoid unwanted distortion in the spatial data. In this experiment, the cameras are oriented more downward on the pavement (Figure 5.7). Also, the traveling speed is reduced to less than 20 mph to reduce the fading effect.

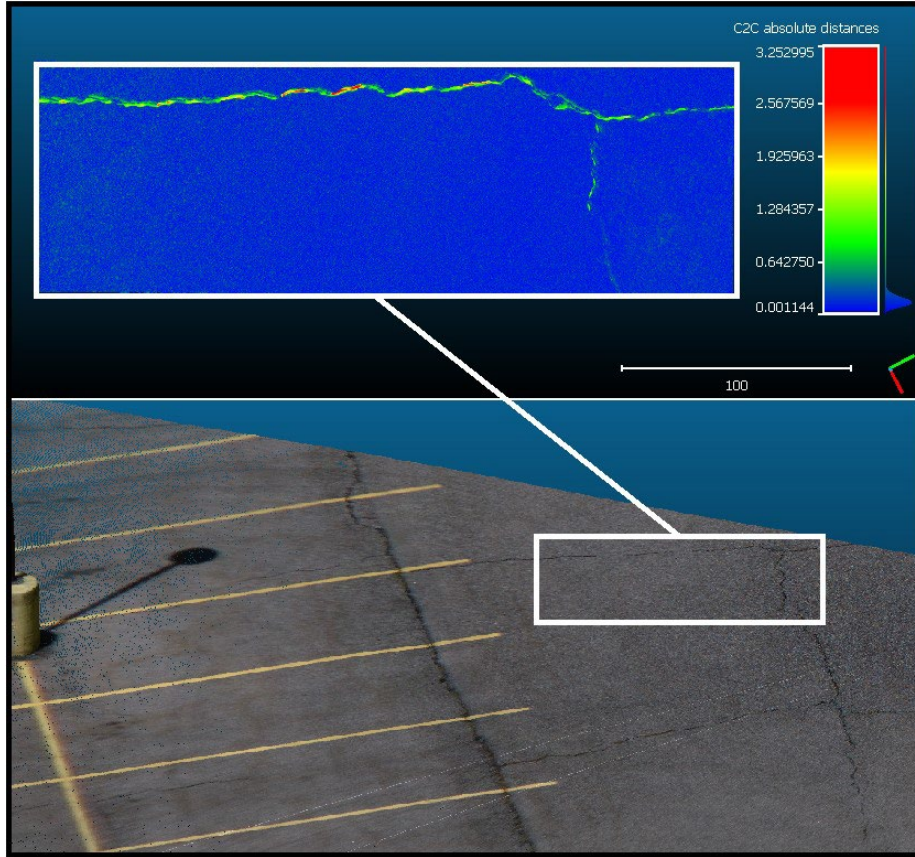


**Figure 5.7** Camera field-of-view of the hood-mounted camera

We used 100 consecutive video frames for this section of the roadway, which was about five meters long. All images are registered in Context Capture on a computer with a 3.20 GHz Intel® Core(i7) CPU, and 64.00 GB of RAM. Image registration and 3D reconstruction took 3 minutes and 31 seconds and 26 minutes and 49 seconds, respectively.

The LiDAR (Maptek I-Site 8820) was set up at a close-range distance from the target pavement distress. This helped us to accurately scan the pavement and have a ground truth model. The laser scanner set up time and scanning time took one hour and 10 minutes.

We used the Cloud Compare software packages to align the two digital point cloud models by registering eight control points. 99.302% of the equivalent pair of points had distances less than 0.436 cm after we registered the two 3D point cloud models. The on-site measurement determined that the target pavement distress had a width in the range of two to four centimeters. The results show a relatively accurate reconstructed pavement distress using mobile photogrammetry, as it is shown in Figure 5.8.



**Figure 5.8** (Bottom) Parking area point cloud, (above) Target pavement distress point-cloud (modeled using LiDAR) to point-cloud (modeled using photogrammetry) (C2C) absolute distances (distances unit in centimeter)

The histogram index demonstrates that there is a maximum deviation of 3.25 centimeters in only small regions inside the crack (red color-coded). However, most of the crack region is only roughly 1 cm deviated from the ground truth model (green color-coded), as it is shown in Figure 5.8.

### 5.2.3 Bridge

The bridge selected for this case study is located at a highway intersection between two highways in the State of Utah, i80 and 215 highways. We collected the video data on a sunny day using a GoPro Hero 8 with a video resolution of 2.7k at 120 frames per second. In this experiment, we were traveling at a speed under 50 mph. The direction of the traveling was also important due to the sunlight reflected from the traffic signs, which may introduce image registration issues. Therefore, consideration must be given to driving direction and time of day while collecting the data. We evaluated the 3D models by measuring the size of the reconstructed bridge structural elements (Figure 5.9).



**Figure 5.9** The target bridge

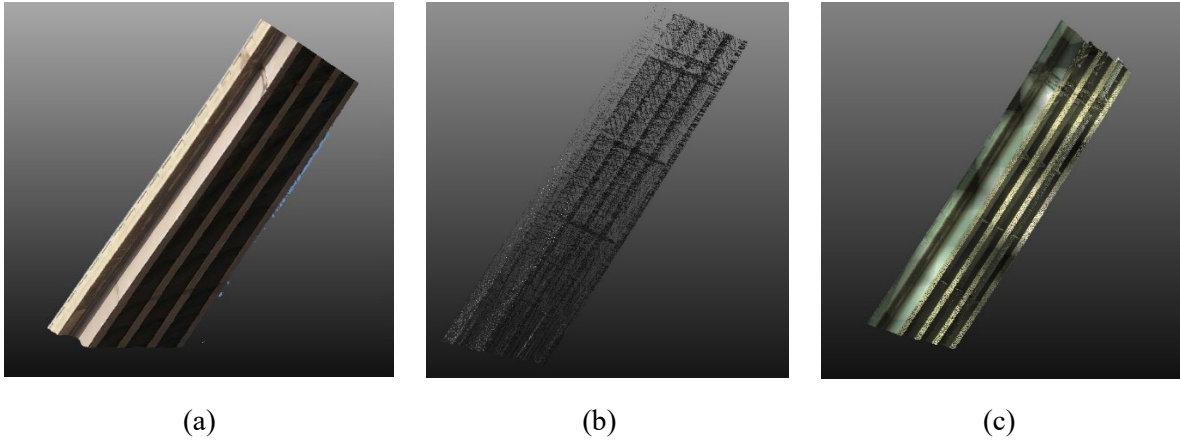
To find the actual measurements of the bridge elements, we needed the as-built drawings. However, there were no available as-built drawing for the selected highway bridge. That said, a terrestrial LiDAR survey was conducted to measure the elements of the target bridge. This portion of the LiDAR model is provided by engineers from the Utah Department of Transportation. They used a Leica C10 in a four-point survey from each corner of the bridge near the abutment wing walls. Figure 5.10 shows the photogrammetric and LiDAR-based reconstructed 3D models of the bridge and its deck-mounted traffic sign.



**Figure 5.10** Map of reconstructed highway sections (showing the bridge model and a traffic sign model). Images are from both LiDAR-based highway models and image-based highway models.

There were a few noticeable differences between the three generated point cloud models of the target bridge. The two LiDAR point cloud models (the ground truth model and the mobile LiDAR model) did not include the small structural bridge details, such as bolts and cracks, but retained all large bridge components, such as girders, columns, and diaphragms. Consequently, the point cloud models are not enough for structural inspection purposes. On the other hand, the photogrammetry 3D model shows the side of the bridge that was in front of the camera sensor in detail. Similar to the LiDAR models, the image-based model was not a clear set of points to inspect the underneath and the backside of the bridge. A second camera on the back of the car may solve this issue.

Also, the sudden changes in illumination cause image registration errors. This error caused a skewness in the reconstructed 3D model. This was due to the fact that the number of image features decreased between the pair of images. In the same way, the number of roadway lanes covered using photogrammetry is reduced from about two lanes far from the camera sensor (in normal lighting conditions) to about one lane far from the camera sensor under the bridge deck regions. The linear accuracy of the spatial data was evaluated by measuring the width to the span length of the bridge at bridge diaphragms, as it is depicted in Figure 5.11. Table 5.5 tabulated the average error percentage of width to span ratios. The error of the mobile LiDAR was in the range of about 1%.



**Figure 5.11** Bridge’s underside in (a) Mobile photogrammetry model, (b) Mobile LiDAR model, (c) Terrestrial LiDAR model

**Table 5.5** Extracted Bridge Span Measurements for Terrestrial and Mobile LiDAR-based Reconstruction

Location	Mobile LiDAR			Terrestrial LiDAR			Percent Error (%)
	Span Length	Span Width	Ratio (W/L)	Span Length	Span Width	Ratio (W/L)	
1	54.84	6.72	0.1225	55.24	6.89	0.1247	1.76
2	54.84	6.76	0.1233	55.24	6.79	0.1229	0.28
3	54.84	6.70	0.1222	55.24	6.78	0.1227	0.46
4	54.84	6.72	0.1225	55.24	6.72	0.1217	0.73
5	54.84	6.69	0.1220	55.24	6.90	0.1249	2.34
6	54.84	6.90	0.1258	55.24	6.72	0.1217	3.43
7	54.84	6.78	0.1236	55.24	6.80	0.1231	0.43
8	54.84	6.79	0.1238	55.24	6.82	0.1235	0.29
9	54.84	6.86	0.1251	55.24	6.74	0.1220	2.52
10	54.84	6.85	0.1249	55.24	6.83	0.1236	1.02
11	54.84	6.77	0.1235	55.24	6.88	0.1245	0.88
Average							1.29

## 5.3 Results of the Terrestrial Collected 3D Data

### 5.3.1 Pedestrian Access Ramp

When evaluating the spatial data created for the pedestrian access ramps, it is important to assess the measurements that are critical in the actual in-field inspections of those ramps. That considered, the most important aspect of assessing the data recorded from pedestrian access ramps is to make sure that the different ramp components are within specifications defined by the Department of Transportation and that their tolerances are met. To that end, we measured the slopes of the different components of the sample ramps and also the distances of those areas to ensure that they were passing per the standards of the department of transportation. In the following sections, we present tables, including measurements that were extracted from the point cloud models of the pedestrian access ramps (tabulated in Table 5.6 and Table 5.7).

**Table 5.6** Pedestrian access ramp slope errors

<b>Pedestrian Access Ramp Model</b>	<b>Technology</b>	<b>Slope Error (%)</b>
Ramp 1	Photogrammetry	0.60
	LiDAR	0.27
Ramp 2	Photogrammetry	0.28
	LiDAR	0.19
Ramp 3	Photogrammetry	0.28
	LiDAR	0.16
Ramp 4	Photogrammetry	0.35
	LiDAR	0.19
Ramp 5	Photogrammetry	0.24
	LiDAR	0.18
Ramp 6	Photogrammetry	0.16
	LiDAR	0.14
<b>Average Error</b>	<b>Photogrammetry</b>	<b>0.32</b>
	<b>LiDAR</b>	<b>0.19</b>
<b>Standard Deviation</b>	<b>Photogrammetry</b>	<b>0.15</b>
	<b>LiDAR</b>	<b>0.04</b>
<b>Coefficient of Variation</b>	<b>Photogrammetry</b>	<b>0.48</b>
	<b>LiDAR</b>	<b>0.24</b>

**Table 5.7** Data Processing Table for Pedestrian Access Ramps












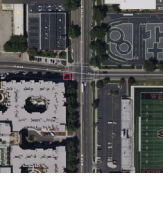
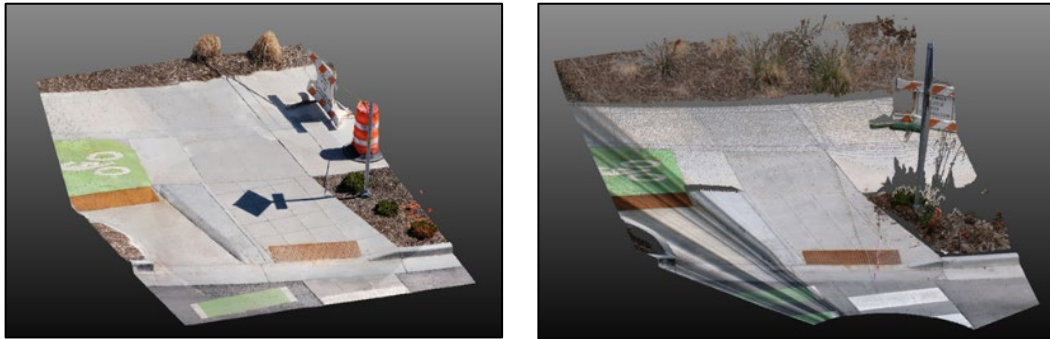
Ramp	Image	Location	Number of Photos	Number of Points	Keypoints	Tie Points	RMS
Ramp 1			31 Photos Total, 31 aligned	258,651,814	Median of 47,166 keypoints per image	Median of 384 tie points per photo	0.69 pixels
Ramp 2			37 Photos total, 37 aligned	429,797,343 (295,559,874 Cleaned)	Median of 46,394 keypoints per image	Median of 162 tie points per image	0.75 pixels
Ramp 3			29 total photos, 27 aligned	313,767,481 (153,790,452 Cleaned)	Median of 46400 keypoints per image	Median of 189 tie points per photo	0.73 pixels
Ramp 4			31 total photos, 31 aligned	264,338,208	Median of 22776 keypoints per image	Median of 524 tie points per photo	0.64 pixels
Ramp 5			29 total photos, 27 aligned	436,552,997 (267,786,121 Cleaned)	Median of 46968 keypoints per image	Median of 125 tie points per photo	0.74 pixels
Ramp 6			25 total photos, 24 aligned	247,958,617 (162,860,993 Cleaned)	Median of 26,733 keypoints per image	Median of 352 tie points per photo	0.63 pixels

Figure 5.12 shows ramp number one in the sample ramps that we modeled. This ramp is located near the University of Utah hospital. The comparison of the measurements from the in-field measurements and virtual measurements from the 3D models resulted in a very negligible error when either of the sensing technologies is used, 0.6% error for photogrammetry and 0.27% error for LiDAR, as it is shown in Figure 5.13.



It is noteworthy that the measurements extracted from the virtual models can be claimed to be even more accurate than the in-field measurements. For example, the flare (a very small component of the ramp) is only about one foot long, and during the in-field inspections, a meter-long level was used to measure the slope of this particular component. Therefore, the measuring device was not a standard device and may result in inaccurate measurements. However, except for that flare, the measurements of the other components (slopes) are very close to the in-field measurements.



(a)

(b)

**Figure 5.12** Ramp 1 point clouds using (a) photogrammetry and (b) LiDAR

**UDOT C-170 Pedestrian Access Evaluation Form**  
 Refer to UDOT 74 Series Standard Drawings for completion requirements  
 March, 2020

Inspector: [Signature] Date: [Date] City: [City] State: [State] County: [County] HSN/Project: [Project Name]

Primary Access: [Location] Secondary Access: [Location]

NOTES:  
 1. If a corner or location has multiple accesses, complete a separate form for each.  
 2. Inventory accesses from the roadway facing the corner/back of access; provide unique and repeatable identifiers  
 3. Construction Violations - all slopes must be within 0.04% of tolerance  
 4. Document substantial sidewalk without an approved Technical Infeasibility. Accesses will not FAIL due to substantial sidewalk.  
 5. Waive compliance to adjacent sidewalk cross slopes within at least one panel.  
 6. Document substantial crosswalks without an approved Technical Infeasibility. Accesses will not FAIL due to substantial crosswalk.  
 \*Cross Slope Criteria: ≤ 2.0% if Controlled by Stop/No-Stop; ≤ 5.0% if not Controlled by Stop/No-Stop (including signals); Max. Road Grade at Midblock

Access Type: Parallel, Curved, At-Grade, Directional

Measurement and Determination (Pass/Fail)

Min. Lined Joints on curb breaks	Yes	No	Pass	Fail	Pass	Fail	Pass	Fail	Pass	Fail
Pedestrian Access Route (PAR)	Width (± 4 ft)	6.7	Pass	Fail	Pass	Fail	Pass	Fail	Pass	Fail
Turning Space (T)	Depth (Minimum of min. Concrete 5' max)	6	Pass	Fail	Pass	Fail	Pass	Fail	Pass	Fail
Ramp (R)	Running Slope (± 0.3%)	0.97	Pass	Fail	Pass	Fail	Pass	Fail	Pass	Fail
Flare (F)	F3 Slope (± 25.0%)	6.04	Pass	Fail	Pass	Fail	Pass	Fail	Pass	Fail
At-Grade Access (A)	Running Slope (± 2.0%)	6.7	Pass	Fail	Pass	Fail	Pass	Fail	Pass	Fail
Thruway Island (TI)	Min. Width (± 4 ft)	6.7	Pass	Fail	Pass	Fail	Pass	Fail	Pass	Fail

(a)

Element	Item (Pass Criterion)	Location	Location	Location	Location	Comments
Detectable Warning Surface (DWS)	Type	Polymer Cast Iron Stamped/ Precast	Polymer Cast Iron Stamped/ Precast	Polymer Cast Iron Stamped/ Precast	Polymer Cast Iron Stamped/ Precast	
	Color Contrasts with Surrounding Surface	Yes	Yes	Yes	Yes	
	Squares Full Curbs Cut (± 4" single, ± 8" dual)	Yes	Yes	Yes	Yes	
	Depth (± 2")	2.7	Pass	No	Pass	Pass
	Theoretical Edge ≤ 5" to TBC or 2" high	Yes	Fail	Yes	Fail	Fail
	Outside Corners 2" from (projected) TBC	Yes	Yes	Yes	Yes	
	Gap Between Brm Multiple Panels (± 2", 0" preferred)	Yes	No	No	No	
	Clear Space (C)	Width of Walk and Outside Travel Lane	1.07	Pass	Pass	Pass
	Slope Perpendicular to DWS (± 5.0%)	1.07	Pass	Pass	Pass	Pass
	Slope Parallel to DWS (± 2.0%)	0.27	Fail	Fail	Fail	Fail
Vertical Difference ± 0.5" or 2:1 beveled	0.27	Yes	No	Yes	No	
Crosswalk (marked or unmarked)	Running Slope (± 5.0%)	1.17	Pass	Pass	Pass	
Cross Slope* (± 2.0%)	6.7	Fail	Fail	Fail	Fail	
Ped/Bush	Height above (T) (42 ± 2", or 36"-46" if RTE approved)	Pass	Pass	Pass	Pass	
Offset from (T) (± 10", 18" max if RTE approved)	Pass	Pass	Pass	Pass	Pass	

Certified UDOT Inspector (Print): [Signature]  
 Certified Contractor (Print): [Signature]

Suggested work to meet Standards (Select all that apply):  
 Re-grade intersection and/or roadway  
 Widen roadway and/or pedestrian facilities  
 Reconstruct adjacent sidewalk or pedestrian facility  
 Purchase right-of-way (acquisition or temporary)  
 Demolish/remove adjacent structure or facility  
 Relocate underground utility  
 Relocate above ground utility  
 Relocate ATM or signal equipment  
 Reconstruct/relocate storm drain  
 Re-designation of historic facility

After project inspection, file in ProjectWise and email to AD.A ramps@utah.gov and FHWA Area Engineer.

(b)

Measurement Comparison					
Element	LIDAR Based Measurements	Image-Based Measurements	UDOT's Measurement	Image-Based Error	LIDAR Based Error
PAR Left (cross)	1.61	0.83	2.10	1.27%	0.49%
PAR Right (Cross)	1.68	0.41	1.90	1.49%	0.22%
Turning space Running	1.94	1.66	1.60	0.06%	0.34%
Turning Space Cross	1.18	0.81	1.60	0.79%	0.42%
Ramp Running	0.98	0.33	0.80	0.47%	0.18%
Ramp Cross	0.34	0.63	0.20	0.43%	0.14%
Left Flare	20.3	22.3	53.0	30.75%	32.71%
Right Flare	16.4	16.1	16.5	0.39%	0.09%
Clear Space perp. To DWS	1.33	1.28	1.00	0.28%	0.33%
Clear Space para. To DWS	0.64	1.12	0.80	0.32%	0.16%
Crosswalk Running	1.62	1.92	1.40	0.52%	0.22%
Crosswalk Cross	1.05	1.34	0.70	0.64%	0.35%
Average Error				0.60%	0.27%

(c)

Figure 5.13 Comparison of UDOT's in-field measurements to measurements extracted from image-based point clouds for Ramp 1. (a) & (b) UDOT C-170 evaluation form, (c) extracted measurements vs. UDOT's measurements

The measurements extracted from ramp number two and ramp number three also showed that the virtual inspection could be accurate. For instance, the overall errors for the third model were 0.28% and 0.16% for the reconstructed models of the photogrammetry product and the LiDAR product, respectively.

We concluded that both of the technologies (photogrammetry and LiDAR) are feasible to conduct an accurate enough data collection procedure for the task of pedestrian access ramps. The overall error for photogrammetry was 0.32%, with an STD of 0.15 and a CV of 0.48. For the laser scanning approach, the overall error was less than the photogrammetry error and was 0.19%, with an STD of 0.04 and a CV of 0.24. The lower CV resulting from the LiDAR technology shows that this technology is more consistent in terms of 3D reconstruction of the pedestrian access ramps.

## 6. CONCLUSIONS

Transportation agencies need to regularly keep records of the existing assets in the transportation infrastructure across the country. Due to the vast reach of transportation assets across the country, it is time-consuming and inaccurate to conduct asset inventory tasks by following traditional and manual fashions. The manual inspections are also expensive — it takes a lot of human resource and time. That said, the engineers have been working on automated and semi-automated methods to help transportation agencies conduct the task of asset inventory in the roadway in their jurisdiction.

Among those automated methods, 3D reconstruction methods stand out for many reasons. First, 3D models can always be used to inspect the assets and not just enumerate them. When they are documented as they are, the documentation is not subject to the opinion of the inspectors. This way, the agencies can recognize the actual deterioration rate of the transportation assets. Second, these models can be stored for a long time, and many other measurements that were not supposed to be measured during the data collection can be calculated. For example, the 3D models of the roadways can be used for measurement of the traffic signs, pavement, and any other highway features of interest.

The abovementioned advantages have motivated many transportation agencies (including the Utah Department of Transportation) to leverage modern technologies, such as LiDAR to create virtual models of their roadways. For instance, Mandli Communication Inc., under their contract with the Utah Department of Transportation, provides them with LiDAR-based point cloud models of the interstate roadways. Although this technology has some advantages, it also comes with many disadvantages and limitations. First, laser scanning technology is expensive. As a result, the asset management divisions would need to ask for extravagant budgets to afford such technologies. Furthermore, smaller transportation agencies cannot afford such expensive technologies. Second, LiDAR requires trained and expert users. These two reasons motivated our research team to develop an affordable and easy-to-use approach for collecting data on the roadways.

That considered, the current project investigated an alternative approach for reconstructing the 3D models of the roadways and transportation assets in the form of point cloud models. The introduced method in this project is photogrammetry. This technology is both cheaper and easier to implement. Therefore, it would also be available for smaller transportation agencies. Nevertheless, the accuracy of the photogrammetry technique is subjected to many factors that can limit its use for civil engineering applications. As a result, this project intended to investigate the feasibility of photogrammetry as an asset management tool for transportation agencies. In doing so, we tested this technology for three different applications as follows:

1. Roadway asset management and maintenance
2. Pedestrian ramp inspection
3. Pavement condition assessment

## 6.1 Challenges and Limitations

The environmental conditions were one of the most important challenges for using photogrammetry and LiDAR technologies. The vision-based algorithms embedded in photogrammetry software packages are very sensitive to reflective surfaces in images. Therefore, extreme illumination conditions (too sunny conditions) may affect the quality of the reconstructed 3D models. Moreover, factors, such as snow, rain, sunlight, and car reflections, can cause problems with reconstruction. If there is too much sunlight during data collection, the light may reflect off of various objects, such as vehicles, items on the road, and highway signs.

One of the biggest limitations of asset management data collections using photogrammetry is the speed of the platform. During our research, we found that we were unable to process any data from videos collected while traveling greater than 50 miles per hour. One of the most important aspects of image alignment during photogrammetry reconstruction is having enough keypoints in each image to be able to have an accurate alignment.

## 6.2 Recommendations

During this project, we experimented with mobile and stationary settings for collecting data using the two abovementioned sensing technologies — photogrammetry and LiDAR. Regarding the first application, we used a car-mounted digital camera and 3D reconstruction software packages to create image-based point cloud models of the roadway assets, including the traffic signs and highway bridges. Our measurement has shown that photogrammetry can be used as an alternative to LiDAR, considering the fact that the data collection platform (car) must drive at much slower speeds compared to the LiDAR platform speed. That said, photogrammetry is the best alternative to LiDAR for inventorying smaller areas (such as city routes). Therefore, the LiDAR technology is a better choice when collecting highway data because the minimum allowable speed at highways is typically more than the suggested traveling speed for the photogrammetry technology (under 50 mph).

Regarding the pedestrian access ramps, our experiments have shown that both LiDAR and photogrammetry can provide accurate tools for creating virtual models of the ramps. The measurements have shown that the errors calculated after comparing the actual measurements (in-field measurements) with the measurements extracted from the digital models are in the range of less than 1% for both LiDAR-based and photogrammetric models. It is also shown that in some cases, digital models can provide even more accurate measurements than in-field measurements. Therefore, we recommend the use of photogrammetry technology for pedestrian access ramps. The virtual models can be used for both quality assessment and measurements of the different components of the ramps (slopes and distances).

Regarding the third application, we investigated if a slow-moving platform (digital camera) can record enough pixel information in the video data to be used as a source of information for reconstructing the pavement distresses. To that end, we conducted our experiment in a no-traffic area (in the parking area of the department of civil and environmental engineering in the University of Utah campus area). This would let us use a stationary laser scanner to collect accurate spatial data from the target pavement distress without the presence of any noise (occlusion of the target area by traffic). The results have shown that the overlaid ground truth and image-based reconstructed models are similar with slightly different depths (more than 90% of the areas with a one centimeter difference). It should be noted that the traveling speed during this experiment was kept under 20 mph. Therefore, further research studies and improvement of the vision-based algorithms are required to enable this application for actual use since the minimum speed at almost most of the roadways exceeds 20 mph. Accordingly, the results of this project are published in [23-26].

Mobile photogrammetry works well in cases where the camera platform can be transported at slower speeds and the assets are not far from the roadway (less than two lanes far away). Therefore, LiDAR may be a better option for faster rates of travel and assets at distances. Considering overall point cloud densities, the authors recommend the use of photogrammetry for pavement distress analysis only on the road lane in which the mobile sensor is located. Moreover, it is predicted that the increased traveling speed could negatively influence pavement deformation 3D reconstruction accuracy. To address the existing gaps in this subject, we recommend the following for future research works:

1. Comparison of the mobile LiDAR and photogrammetry in pavement distress condition assessment.
2. A comprehensive sensitivity analysis of the different traveling speeds' effect on the quality and the precision of the 3D reconstructed point clouds.
3. Assessment of the Unmanned Aerial Vehicle (UAV) photogrammetry and LiDAR systems on highway asset management along with the mobile LiDAR to fill the gaps that mobile LiDAR cannot access.
4. Using multiple cameras to be able to increase the traveling speed at which the data is collected.

## REFERENCES

1. U.S. Department of Transportation; Federal Highway Administration (FHWA): Safety, 2020. <https://safety.fhwa.dot.gov/> Accessed May 15, 2020
2. Highway Maintenance Manual (HMM) 02-10-15 Maintenance Definitions. 2017. <https://wisconsindot.gov/Documents/doing-bus/local-gov/hwy-mnt/mntc-manual/chapter02/02-10-15.pdf> Accessed May 15, 2020
3. Mashhadi AH, Farhadmanesh M, Rashidi A, Marković N. State-of-the-Art Methods in Estimating Freeway Work zones Capacity: A Literature Review. Transportation Research Board 100th Annual Meeting Transportation Research Board. 2021(TRBAM-21-01863).
4. Ellsworth P. Utah DOT leveraging LiDAR for leap to asset management. *LiDAR Art of the Scan*. 2013;3(1):38-43.
5. Ai C, Hou Q. Improving Pedestrian Infrastructure Inventory in Massachusetts Using Mobile LiDAR. 2019 Sep.
6. Mandli, “Utah DOT: The Blueprint,” 2012. [Online]. Available: <https://www.mandli.com/wp-content/uploads/2016/02/Utah-DOT-Blueprint.pdf>.
7. L. Klein, N. Li, and B. Becerik-Gerber, “Imaged-based verification of as-built documentation of operational buildings,” *Autom. Constr.*, vol. 21, pp. 161–171, 2012.
8. S. Chae and N. Kano, “Application of location information by stereo camera images to project progress monitoring,” in *Proceedings of the 24th International Symposium on Automation and Robotics in Construction, Kochi, Kerala, India, 2007*, pp. 19–21.
9. S. Gordon, D. D. Lichti, M. P. Stewart, and M. Tsakiri, “Metric performance of a high-resolution laser scanner,” in *Videometrics and Optical Methods for 3D Shape Measurement, 2000*, vol. 4309, pp. 174–184.
10. C. Tucker, “Testing and verification of the accuracy of 3D laser scanning data,” in *Symposium on geospatial theory, Processing and Applications, Ottawa, 2002*.
11. J. Clark and S. Robson, “Accuracy of measurements made with a Cyrax 2500 laser scanner against surfaces of known colour,” *Surv. Rev.*, vol. 37, no. 294, pp. 626–638, 2004.
12. D. D. Lichti and B. R. Harvey, “The effects of reflecting surface material properties on time-of-flight laser scanner measurements,” *tc*, vol. 2, p. 1, 2002.
13. T. Voegtle and S. Wakaluk, “Effects on the measurements of the terrestrial laser scanner HDS 6000 (Leica) caused by different object materials,” *Proc. ISPRS Work*, vol. 38, no. 2009, pp. 68–74, 2009.
14. Z. Zhou, J. Gong, and M. Guo, “Image-based 3D reconstruction for posthurricane residential building damage assessment,” *J. Comput. Civ. Eng.*, vol. 30, no. 2, p. 4015015, 2016.
15. A. Bhatla, S. Y. Choe, O. Fierro, and F. Leite, “Evaluation of accuracy of as-built 3D modeling from photos taken by handheld digital cameras,” *Autom. Constr.*, vol. 28, pp. 116–127, 2012.

16. H. Fathi, F. Dai, and M. Lourakis, “Automated as-built 3D reconstruction of civil infrastructure using computer vision: Achievements, opportunities, and challenges,” *Adv. Eng. Informatics*, vol. 29, no. 2, pp. 149–161, 2015.
17. L. Klein, N. Li, and B. Becerik-Gerber, “Imaged-based verification of as-built documentation of operational buildings,” *Autom. Constr.*, vol. 21, pp. 161–171, 2012.
18. M. Pollefeys et al., “Detailed real-time urban 3d reconstruction from video,” *Int. J. Comput. Vis.*, vol. 78, no. 2–3, pp. 143–167, 2008.
19. I. Brilakis, H. Fathi, and A. Rashidi, “Progressive 3D reconstruction of infrastructure with videogrammetry,” *Autom. Constr.*, vol. 20, no. 7, pp. 884–895, 2011.
20. A. Rashidi, F. Dai, I. Brilakis, and P. Vela, “Optimized selection of key frames for monocular videogrammetric surveying of civil infrastructure,” *Adv. Eng. Informatics*, vol. 27, no. 2, pp. 270–282, 2013.
21. M. Lato, M. Diederichs, “Mapping Shotcrete Thickness using LiDAR and Photogrammetry Data: Correcting for Over-Calculation due to Rockmass Convergence.” 2014.
22. D. Veneziano, R. Souleyrette, S. Hallmark, “Integrating LiDAR and Photogrammetry in Highway Location and Design.” 2003.
23. Farhadmanesh, M., Cross, C., Mashhadi, A. H., Rashidi, A., & Wempen, J. (2021). Highway asset and pavement condition management using mobile photogrammetry. *Transportation Research Record*, 2675(9), 296-307.
24. Farhadmanesh, M., Cross, C., Mashhadi, A. H., Rashidi, A., & Wempen, J. (2021). Use of mobile photogrammetry method for highway asset management. In *100th Annual Meeting of the Transportation Research Board, Washington, DC*.
25. Cross, C., Farhadmanesh, M., & Rashidi, A. (2020). *Assessing Close-Range Photogrammetry as an Alternative for LiDAR Technology at UDOT Divisions* (No. UT-20.18). Utah. Dept. of Transportation. Division of Research.
26. Farhadmanesh, M., Cross, C., Rashidi, A., & Wempen, J. (2022). Feasibility Study of Using Close-Range Photogrammetry as An Asset Inventory Tool at Public Transportation Agencies. *ASCE Journal of Performance of Constructed Facilities*.